

**OPERATIONAL PARAMETERS OPTIMIZATION OF CROSS-FLOW  
CERAMIC MEMBRANE ULTRAFILTRATION FOR WATER  
DEPYROGENATION**

by

Orlando Sifre-González

A project submitted in partial  
fulfillment of the requirements for the  
degree of

MASTER OF ENGINEERING

in

Chemical Engineering

UNIVERSITY OF PUERTO RICO

MAYAGUEZ CAMPUS

2004

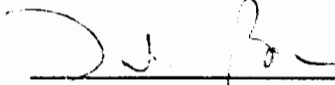
Approved by:



Jaime Benítez Rodríguez, Ph.D.  
Member, Graduate Committee

4/26/04

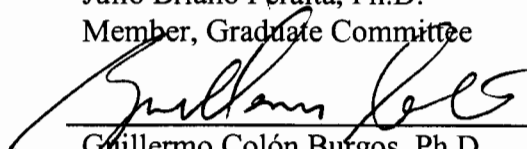
Date



Julio Briano Peralta, Ph.D.  
Member, Graduate Committee

4/26/04

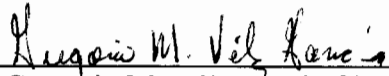
Date



Guillermo Colón Burgos, Ph.D.  
President, Graduate Committee

4/26/04

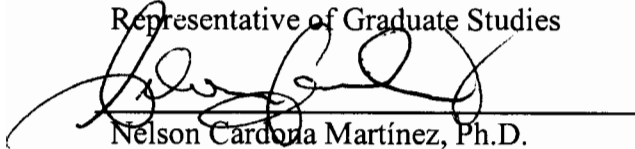
Date



Gregorio M. Vélez, M.S. Ch.E.  
Representative of Graduate Studies

4/26/04

Date



Nelson Cardona Martínez, Ph.D.  
Chairman of Ch.E. Department

4/28/04

Date



Jose Mari Mutt, Ph.D.  
Director of Graduate Studies

5/5/04

Date

## ABSTRACT

Water ultrafiltration has been suggested as an alternative for the removal of lypopolysaccharides in the production of Water for Injection and, Pyrogen Reduced Water. Ultrafiltration of water using an annular ceramic membrane with nominal molecular weight cut off  $< 50,000$ , has been confirmed as a viable choice for the production of such water types, producing filtrates of pyrogenic concentration below 0.03 EU/mL at permeate rates of up to  $775 \text{ L/m}^2\text{-hr}$ . Operational parameters like endotoxin feed concentration, feed rate and transmembrane pressure were assessed utilizing a factorial experimental design. The flux profiles obtained showed a linear relationship with transmembrane pressure up to the maximum concentrations studied of 667 EU/mL. Statistical evidence revealed that the permeate flux response is proportionally determined by the feed rate and transmembrane pressure main factors and the interaction of them. The endotoxin concentration was statistically identified as a non-significant factor affecting permeates flux.

## RESUMEN

El proceso de ultrafiltración de agua ha sido sugerido como una tecnología alterna para la remoción de lipopolisacáridos en la producción de agua para inyección y de agua con un contenido reducido de pirogenos. En este trabajo fue confirmado que la ultrafiltración de agua utilizando una membrana anular de cerámica con un tamaño de retención molecular de  $< 50,000$  es una opción viable para la producción de los tipos de aguas mencionados, generando filtrados de una concentración pirogenica menor a 0.03 EU/mL obteniendo un flujo de filtración de hasta  $775 \text{ L/m}^2\text{-hr}$ . Los parámetros operacionales como la concentración de endotoxinas, el flujo volumétrico y la presión a través de la membrana fueron estudiados utilizando un diseño experimental factorial. Los perfiles de flujo obtenidos exhibieron una relación lineal con la presión transmembránica hasta una máxima concentración estudiada de 667 EU/mL. La evidencia estadística reveló que la respuesta del flujo de permeato está determinada proporcionalmente por los factores principales de flujo volumétrico y la presión transmembránica y la interacción de los mismos. La concentración de endotoxinas fue identificada estadísticamente como un factor no-significativo que afecte el flujo de permeato.

## **DEDICATION**

This work is dedicated to my wife Myris Elizabeth Acosta Lizardo. Her love demonstrated through her patience and continuous motivation enabled me to complete this work. In the process, she brought to the world the most precious gift I will ever receive, my daughter Niliarys Valeria. That whomever reads, refers or glimpses this work, shall also acknowledge that the sole motivation for its completion was the presence of Myris in my life. To her, I dedicate this project write-up with all my love.

## **ACKNOWLEDGEMENTS**

Hereby would like to recognize the financial aid provided by the Technical Operations Department at Merck Sharp & Dohme in Barceloneta, Puerto Rico. My gratefulness to the current Plant Manager Mr. Edwin Rodríguez, who granted the authorization for the payment for the rental of the pilot unit used in this investigation. Would also like to thank the contributions made by Dr. Guillermo Colon-Burgos, who provided the scientific guidance for the completion of this document and the overall investigation and, to Mr. Gregorio Velez who provided personal and technical support through the entire compilation process of this script. Finally, and most importantly, thanks to God Almighty who has provided the strength, knowledge and endurance necessary for the completion of this endeavor.

## TABLE OF CONTENTS

I. INTRODUCTION.....	1
II. REVIEW OF LITERATURE .....	7
A. Pyrogen Characterization.....	7
B. Case Study: Validation of a ceramic membrane ultrafilter to produce WFI.....	8
C. Case Study: Ultrafiltration in the Production of Pyrogen-Free Water.....	9
D. System Design.....	11
E. Factors Limiting Flux.....	12
F. Mathematical models review.....	16
III. MATERIALS AND PROCEDURES .....	22
A. Batch mode ultrafiltration.....	22
B. Endotoxins and Limulus Amebocyte Lysate (LAL) assay .....	29
C. Cleaning and Sterilization in Place.....	31
IV. RESULTS AND DISCUSSION .....	34
A. Pure water results.....	34
B. Constant endotoxin concentration results .....	40
1. 100 EU/mL Feed Concentration .....	40
2. 500 EU/mL Endotoxin Cbncentration .....	44
3. 667 EU/mL Endotoxin Concentration .....	47
C. Statistical Analysis.....	54
V. CONCLUSION.....	57
VI. RECOMMENDATIONS .....	60
VII. BIBLIOGRAPHY.....	62
APPENDIX.....	64

**LIST OF TABLES**

Table I.1. Limits for Pyrogen Reduced Water .....	3
Table III.1 Ancillary equipment to USFilter's 1T1 bench top pilot unit.....	25
Table III.2 Ultrafiltration element characteristics. ....	26
Table IV.1: Calculated Membrane Resistance at Different Flow Regions.....	38
Table IV.2: Estimated Osmotic Pressure at Various Bulk Concentrations .....	53

## LIST OF FIGURES

Figure I.1 Cross Section of Typical Ceramic Membrane. ....	2
Figure II.1 Solute Transport Across a Membrane .....	14
Figure III.1 Bench-top Pilot Unit (by U.S.Filter Co.).....	23
Figure III.2 Flow Diagram of Experimental System .....	24
Figure IV.1: Averaged results obtained for water with < 0.03 EU/mL grouped in $N_{Re}$ regions and enclosed by the corresponding standard error bars. ....	36
Figure IV.2 Probability plot of standard errors for water with < 0.03 EU/mL, grouped by $N_{Re}$ .....	37
Figure IV.3. Influence of $P_{TM}$ ohe Calculated $R_m$ Profile. ....	39
Figure IV.4: Averaged results obtained for water with 100 EU/mL grouped in $N_{Re}$ regions and enclosed by the corresponding standard error bars. ....	42
Figure IV.5: Probability plot of standard errors for water with 100 EU/mL, grouped by $N_{Re}$ .....	43
Figure IV.6: Averaged results obtained for water with 500 EU/mL grouped in $N_{Re}$ regions and enclosed by the corresponding standard error bars. ....	45
Figure IV.7: Probability plot of standard errors for water with 500 EU/mL, grouped by $N_{Re}$ .....	46
Figure IV.8: Averaged results obtained for water with 667 EU/mL grouped in $N_{Re}$ regions and enclosed by the corresponding standard error bars. ....	49
Figure IV.9. Probability plot of standard errors for water with 667 EU/mL, grouped by $N_{Re}$ .....	50

## LIST OF APPENDIX

Appendix 1. Design parameters for the Membralox® experimental element as provided by vendor literature.....	64
Appendix 2. Flow rates studied and the corresponding Reynolds # for the Membralox® experimental element.....	65
Appendix 3. Permeate flux raw data for < 0.03 EU/mL water.....	66
Appendix 4. Average permeate flux results and Standard Error (SE) in L/(m <sup>2</sup> .hr) for < 0.03 EU/mL water at 25-30 °C.....	67
Appendix 5. Permeate flux raw data for 100 EU/mL water (Data set No. 1).....	68
Appendix 6. Permeate flux raw data for 100 EU/mL water (Data set No. 2).....	69
Appendix 7. Averaged permeate flux results and standard errors (SE) in L/(m <sup>2</sup> .hr) for 100 EU/mL water at 25-30 °C for different flow regions.....	70
Appendix 8. Permeate flux raw data for 500 EU/mL water (Data set No. 1).....	71
Appendix 9. Permeate flux raw data for 500 EU/mL water (Data set No. 2).....	72
Appendix 10. Averaged permeate flux results and standard error (SE) in L/(m <sup>2</sup> .hr) for 500 EU/mL water at 25-30 °C for different flow regions.....	73
Appendix 11. Permeate flux raw data for 667 EU/mL water (Data set No. 1).....	74
Appendix 12. Permeate flux raw data for 667 EU/mL water (Data set No. 2).....	75
Appendix 13. Averaged permeate flux results and standard error (SE) in L/(m <sup>2</sup> .hr) for 667 EU/mL water at 25-30 °C for different flow regions.....	76
Appendix 14. Two-Sample T-Test of Membrane Resistance at the Laminar and Transition Reynolds Regions.....	77
Appendix 15. Two-way ANOVA of the Membrane Resistance with Pressure and Flow Region Factors .....	78
Appendix 16. Linear regression results for <0.03 EU/mL feed concentration at laminar flow rate.....	79
Appendix 17. Linear regression results for 100 EU/mL feed concentration.....	81
Appendix 18. Linear regression results for 500 EU/mL feed concentration.....	83
Appendix 19. Linear regression results for 667 EU/mL feed concentration.....	85
Appendix 20. Linear regression results for 667 EU/mL feed concentration .....	87
Appendix 21. Permeate flux data grouped for P <sub>TM</sub> of 5 psig .....	89
Appendix 22. Two-Factor ANOVA results for P <sub>TM</sub> of 5 psig .....	90
Appendix 23. Permeate flux data grouped for P <sub>TM</sub> =5 psig .....	91
Appendix 24. Results of a Two-Factor ANOVA with replications for P <sub>TM</sub> = 5 psig .....	92
Appendix 25. Permeate flux data grouped for P <sub>TM</sub> = 25 psig .....	93
Appendix 26. Two-Factor ANOVA results for P <sub>TM</sub> = 25 psig .....	94
Appendix 27. Permeate flux data grouped for P <sub>TM</sub> = 25 psig .....	96
Appendix 28. Results of a Two-Factor ANOVA with replications for P <sub>TM</sub> = 25 psig .....	96
Appendix 29. Permeate flux data grouped for P <sub>TM</sub> = 50 psig .....	97
Appendix 30. Results of a Two-Factor ANOVA with replications for P <sub>TM</sub> = 50 psig .....	98

## LIST OF SYMBOLS

$\varepsilon$	porosity of concentration layer or void fraction	
$\delta$	boundary layer thickness	m
$\sigma$	rejection coefficient	
$\Delta\pi$	osmotic pressure across the membrane	Pa or psig
$\eta_0$	viscosity of the solvent in	Pa-s
$d_s$	diameter of solute particle	m
$\pi_m$	osmotic pressure at the membrane	Pa or psig
$v_0$	partial specific volume of solvent	m <sup>3</sup> /kg
$v_1$	partial specific volume of solute	m <sup>3</sup> /kg
$A$	membrane filtration area	m <sup>2</sup>
$C_{(\delta-x)}$	concentration across the film thickness	kg/m <sup>3</sup> or EU/mL
$C_b$	bulk or feed concentration	kg/m <sup>3</sup> or EU/mL
$C_{bl}$	boundary layer concentration	kg/m <sup>3</sup> or EU/mL
$C_p$	permeate concentration	kg/m <sup>3</sup> or EU/mL
$C_s$	solute concentration	kg/m <sup>3</sup> or EU/mL
$D$	diffusion coefficient	m <sup>2</sup> /sec
$J_v$	permeate flux	l/(m <sup>2</sup> -hr)
$J_w$	clean water flux	l/(m <sup>2</sup> -hr)
$M_s$	solute molecular weight	kg/kmol or Daltons
$P_{TM}$	Transmembrane pressure	Pa or psig
$R$	gas constant	
$R_{obs}$	observed retention	
$s (C)$	sedimentation coefficient	sec
$T$	absolute temperature	K
$V_p$	permeate volume	m <sup>3</sup>
$r_{bl}$	specific boundary layer resistance	m <sup>-2</sup>
$R_{bl}$	boundary layer resistance	m <sup>-1</sup>
$R_m$	membrane resistance	m <sup>-1</sup>
$x$	coordinate of solute transport	m

## I. INTRODUCTION

Together with reverse osmosis (RO), ultrafiltration (UF) constitutes a molecular separation process that does not involve a phase change or interphase mass transfer. In its simplest definition, UF is a fractionation technique that can simultaneously concentrate macromolecules or colloidal substances in process streams. Its separation capability covers from the upper side of the ionic range well into the macromolecular range, this is, from 0.001 to 0.02  $\mu\text{m}$ .

In its most basic form it merely consists of pumping the feed solution under pressure over the surface of a suitably supported membrane, of the appropriate chemical nature and in the optimum physical configuration (Cheryan, 1986). Historically, UF has been used to concentrate process streams using recirculation. Currently, applications range from cheesemaking and whey recovery, in the food industry, to the biotechnology-oriented applications such as the harvesting of microbial cells, and fractionation of enzymatic and fermentation processes (Cheryan, 1986).

Traditionally, ultrafiltration membranes have been constructed out of polymeric materials conformed into a supporting or backing structure under the selective zone. Recently, ceramics have been used in the manufacture of UF membranes using the same two zone arrangement. These membranes are formed by the deposition of inorganic solutes such as zirconium oxide, over sintered microporous supports, typically alumina. Some manufacturers claim that specific surface treatments may be applied on the membrane's surface for specialized performance needs. These membranes possess a high

degree of resistance to chemical and abrasion degradation, and tolerate a wide range of pH and temperature. A cross section of such membrane can be appreciated in Figure I.1.

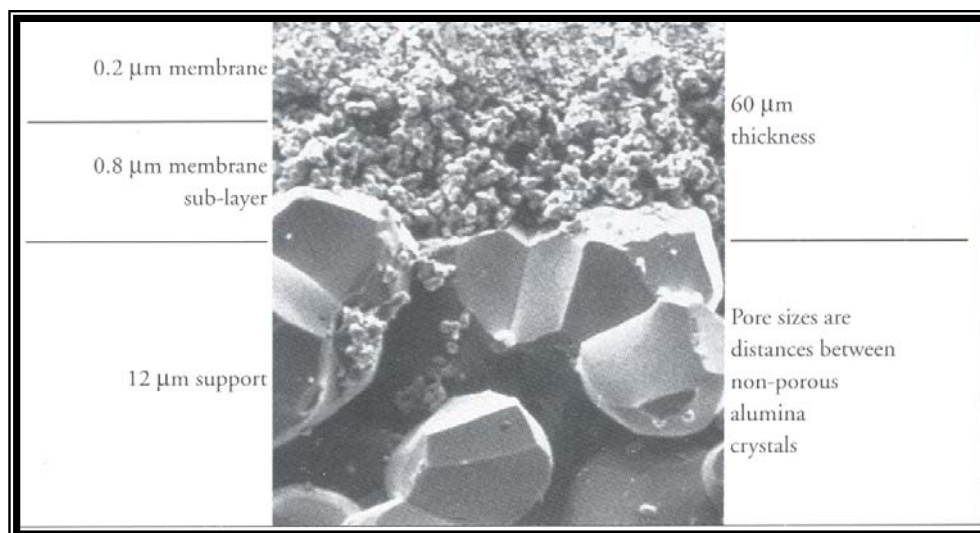


Figure I.1 Cross Section of Typical Ceramic Membrane, taken from US Filters Co., 1997.

Ceramic membrane ultrafiltration has recently been introduced by membrane manufacturers, such as U.S. Filters and Consler Corporation, as a possible alternative to the traditional energy-intensive distillation for the production of pyrogen reduced water. As defined by the United States Pharmacopoeia, pyrogen reduced water (PRW) exhibits the limits established in Table I.1. This type of water is actually a Food and Drug Administration (FDA) requisite for bulk chemical processes as well as for other parenteral products. Currently, distillation and RO are the only technologies approved by the FDA and recommended by the United States Pharmacopoeia, for the production of this type of water.

Type	Limit
Pyrogens	<0.25 EU/mL
Microbes	<100 CFU/mL
Chloride	<2.0 mg/L
Sulfate (as SO <sub>4</sub> )	<4.0 mg/L
Total Sulfides	<10.0 mg/L
Ammonia (as NH <sub>3</sub> )	<0.3 mg/L
Calcium	<4.0 mg/L
Carbon Dioxide @ 25°C	<5.0 mg/L
Heavy Metals	<1.0 mg/L
Oxidizable Substances	<0.8 mg/L
Total Solids	<10.0 mg/L
PH	5.0-7.0

Table I.1. Limits for Pyrogen Reduced Water, taken from Parekh, B. S. 1991.

When compared to distillation, ceramic membrane systems have low operating costs because of their small utility requirements, as well as substantial outputs depending on the membrane surface area. The total costs, i.e., installation, operation, maintenance, and power consumption, of a distillation process has been reported as \$94 per thousand gallons produced, while for UF and RO, costs have been reported as \$26.50 per thousand gallons produced (Parekh, 1991). Advantages of UF over other water purification techniques are:

1. UF ceramic membranes allow for sterilization and cleaning versatility in contrast to polymeric RO membranes.
2. A change in phase or state of the solvent during the dewatering process requiring large energy inputs is not necessary. Evaporation requires 1000 BTU/Lb. of water (Cheryan, 1986).

3. Neither condensers nor the huge condenser cooling water supply required for their operation are needed, thus avoiding related problems like thermal pollution and overloading of sewage treatment systems.
4. UF processes can be operated at ambient temperatures, avoiding thermal or oxidative degradation problems common to evaporation processes.
5. Minimal changes occur in the microenvironment during UF since small molecules should freely pass through the membranes. This causes the concentration of these components on either side of the membrane to be the same and equal to the original feed concentration (No pH or ionic strength change).

On the other hand some of the limitations of UF systems are:

1. Membrane processes are limited in their upper solid limits. In the case of UF, the low mass transfer rates obtained with concentrated macromolecules, and the high viscosity that makes pumping of the retentate difficult, limit the process.
2. Fouling, poor cleanability and restrictive operating conditions inhibit process optimization.

The mentioned benefits are well known to process engineers, leading to the execution of validation exercises that document the feasibility of the technology for different applications, such as the production of Water for Injection (WFI) (Engel, et. al., 1992). Validation studies cover process variable ranges pertinent to the current stipulations of a particular process. Taking this into account, the information obtained from such a study is limited to determining the feasibility of a particular application.

However, to understand the capabilities of this new technology: Ultrafiltration using ceramic membranes to produce PRW, a full study is recommended.

The reliability of water ultrafiltration to produce PRW in the long term and, its performance upon variations in the feed characteristics or production requirements of PRW, are aspects necessary to be understood prior to challenging the system with further applications. This suggests that a designed experimental study to assess the ultrafiltration technology using ceramic membranes to produce PRW is pertinent and necessary. Special attention has to be given to the mentioned limitations of ultrafiltration, to thoroughly describe the intended application.

The general objective of this investigation was to study the interaction of the operating parameters of a laboratory scale prototype, which resembles a water ultrafiltration system model and their effect on membrane flux performance. This research served to determine the feasibility of the production of pyrogen reduced water using ceramic membrane ultrafiltration, and provided data to be compared against mathematical models. This purpose was accomplished fulfilling the following detailed objectives:

1. Investigated the production of PRW using a ceramic membrane made of zirconia deposited over alumina of molecular weight cut-off size of 10,000.
2. Established the statistical comparisons of permeate flux performance for various endotoxin feed concentrations and using different feed rates covering all flow regions.

In addition, the transport phenomena characterizing permeate flux was qualitatively associated to experimental results.

## II. REVIEW OF LITERATURE

### A. Pyrogen Characterization

Pyrogens are defined as any substance that causes a temperature rise in humans when injected (Cheryan, 1986). These high-molecular-weight molecules range from 20,000 Daltons to aggregates of 0.1  $\mu\text{m}$ . In their majority Pyrogens are lipopolysaccharides (a polysaccharide portion covalently bounded to a lipid A) derived from the cell walls of gram-negative bacteria. Because the lipopolysaccharides molecules contain both hydrophobic and hydrophilic regions, they form micelle-like aggregates.

Characterized as endotoxins, lipopolysaccharides (LPS) are released from the bacterial surface when bacteria die or replicate. Once they are free inside a living organism, they can either bind to circulating proteins, which trigger the production of immune cells and mediators, or to other receptors on immune cells, therefore alerting the host's defenses of possible pathogenic invaders. When LPS concentrations are extremely high, excessive amount of mediators may be produced, becoming toxic to host cells. During cellular interaction, lipid A, which represents the toxic center of LPS, adopts a peculiar conformation responsible for its characteristic biological activities.

Lipopolysaccharide's threshold of detectability is 0.01-0.1 ng/mL, using the Limulus Amebocyte Lysate (LAL) method, as required by the 4<sup>th</sup> Supplement, Addendum a, of the United States Pharmacopeia-NF. This method is credited to Drs. Bang and Levin, Johns Hopkins' scientists from the Marine Biological Laboratories in

Woods Hole, MA during the 1960's. Autoclaving or microfiltration cannot eliminate these substances, leading to the investigation of alternative techniques such as distillation, and the less energy demanding, ultrafiltration. Companies, such as Amicon, have claimed to reduce pyrogen levels using polymeric membranes of 10,000 molecular weight cut off to levels below 0.050 ng/mL consistently for up to 15 days of pyrogenic challenges.

### **B. Case Study: Validation of a ceramic membrane ultrafilter to produce WFI**

Aleks Engel and Vivian Cheung, from the Massachusetts Institute of Technology performed a validation study in 1994 at the West Point facilities of Merck Sharp & Dohme, for the production of WFI using ceramic membranes. Endotoxin requisites for WFI and PRW are the same, that is <0.25 EU/mL. In this study, deionized feed water was used in a 3.8 m<sup>2</sup> surface area module equipped with the 200 Å MEMBRALOX<sup>®</sup> ceramic membranes manufactured by U. S. Filters. This system was operated in open loop. Results were obtained for Sterilization in Place (SIP) tests, Cleaning in Place (CIP) cycles, and the corresponding WFI assay.

Particularly, the system was challenged with various feed concentrations of LPS ranging from 1.08 to 29105 EU/mL. The system produced WFI satisfactorily with less than 0.25 EU/mL, for LPS feed concentrations of less than 7519 EU/mL, although unsatisfactory results were obtained with feed concentrations of 4140 EU/mL. These results were not correlated to operational parameters such as trans-membrane pressure, due to equipment limitations, nor to mathematical or hydraulic models. Observations

regarding permeate flux proportionality with temperature, shear rate effects on LPS deposition, and purge ratio calculations, were addressed among other topics. It was concluded, in the study, that the purging ratio of the system should be high enough to ensure manageable pyrogen concentrations in the recycle.

Sterilization using steam at 29 psig for 38 minutes was found to be effective on reducing microbial population. Finally, CIP was found ineffective when a solution of sodium borate, citric acid and sodium hypochloride was used, while effective cleaning, or pyrogen reduction, was found when sodium hydroxide and sodium hypochloride were used as the cleaning agents. No cleaning frequency was determined since no fouling studies were performed.

### **C. Case Study: Ultrafiltration in the Production of Pyrogen-Free Water**

A three-year study conducted by Japan's Ministry of Health and Welfare demonstrated the ability of double-skinned polysulfone UF membranes with 6000 dalton molecular weight cut-off, rating to consistently and reliably remove endotoxin to detection level (Kunihiro, 1989). Various challenges were conducted including high temperature endotoxin challenges of up to 29 EU/mL in a recirculation system. No endotoxin was detected in the permeate while operating at 80 °C.

A second challenge included endotoxin levels of  $6.8 \times 10^3$  EU/mL for a retentate-recirculating system operating close to ambient temperature. LAL tests could not detect endotoxins in the permeate at a sensitivity of 0.125 EU/mL. Additional endotoxin challenges, such as a 2000 hour operation at ambient temperature, and a six month run

spiked with both endotoxins and bacteria ranging from  $10^5$  to  $10^9$  cfu/mL, resulted in no detection of endotoxins in the permeate (Krygier, 1997).

#### **D. System Design**

There exist three basic operating modes for UF systems. These are the single pass mode, the batch-recirculation mode, and the feed and bleed mode. The single pass mode can be used on relatively pure water streams such as deionized water, and can produce as much as 95 to 99% permeate recovery if the retained species are low in concentration. It is sometimes advantageous to operate various single pass UF modules in series to maintain a longer contact time with the membranes and to reduce the volumetric pumping requirements.

However, even with single pass modes in series, the permeate flux in most cases is too low to operate, or a desired retentate concentration is difficult to obtain. Therefore, recirculation of the process stream across the membrane is necessary to obtain the desired ultrafiltration results. The limitations of the single pass mode motivate alternative operational modes, namely batch operating mode and the feed and bleed mode.

In the batch-recirculation mode the retentate is returned to the feed reservoir. As the permeate is removed, the concentration of the retained species increases while the volume of the retentate decreases, until a desired concentration is reached. On the other hand, the feed and bleed mode permits continuous filtration and allows increase in concentration of retained species. The increase in concentration of retained species is achieved according to the control established to the feed to bleed ratio. This suggests that if the feed and bleed ratio is the same to a specified concentration ratio, the desired bleed concentration may remain constant even with decreasing permeate flux.

Often, arranging the system into various stages can reduce the total membrane area in a feed and bleed mode. For these “cascade” arrangements, the bleed of one stage becomes the feed of the next one, and so on. For each of these stages there is an optimum recirculation rate. In general, higher recirculation rates results in larger fluxes, less membrane area, and longer membrane life due to greater flux stability (Porter, 1990). It should be noticed that the optimum flow rates at the different stages might differ from one another because of concentration polarization (see section 2.4 Factors Limiting Flux) upon increasing concentration. Therefore, high flow fluid velocities are not as critical for initial stages as for later ones, suggesting that the operating pressure is the critical parameter at these initial stages.

Several designs have been developed in order to determine the most effective membrane arrangement for a concentration or separation process. These are similar to the distillation column design principle of an “equilibrium curve”. However, instead of relying on the thermodynamic equilibrium of the species, the design curve represents the separation characteristics of the particular stage. In general, the separation characteristics are a function of: the selectivity of the membrane, the fluid dynamics of the module, the driving force, the concentration level, and the flow pattern inside the modules, this is, either co-current or counter-current flow.

### **E. Factors Limiting Flux**

It has been well documented that regardless of module design optimization, or specialized membrane properties for any particular application, flux decline is inevitable. This event is observed when the system pressure increase, the convective transport of

solutes toward the membrane increases, creating what is named “concentration polarization (CP)”. CP results in a localized increase in concentration of solute at the membrane surface and lowers the flux due to either high osmotic pressure (Ilias, 1989), the size of the retained molecules, or to the formation of a resistive dynamic layer, resulting in a decrease of the driving force. At the steady-state conditions the convective transport to the membrane must equal the back-diffusive transport away from the membrane. However, the system may overcome these conditions due to an increase in the bulk concentration, which drives the transport net effect towards the membrane surface and enhancing the chance of concentration polarization and even fouling of the membrane.

Nevertheless, concentration polarization effects are reversible. Thus, decreasing the trans-membrane pressure, or lowering the feed concentration can reduce its effects. In addition, by altering the hydrodynamics of the flow, back diffusion from the concentrated boundary layer towards the bulk, can be promoted (see Figure II.1).

Fouling effects, on the other hand, are characterized by an irreversible decline in flux. The general opinion is that fouling is due to deposition and accumulation of sub-micron particles on the membrane surface and/or crystallization and precipitation or adsorption of smaller solutes and macromolecules on the surface and within the pores of membrane itself (Ilias, 1989).

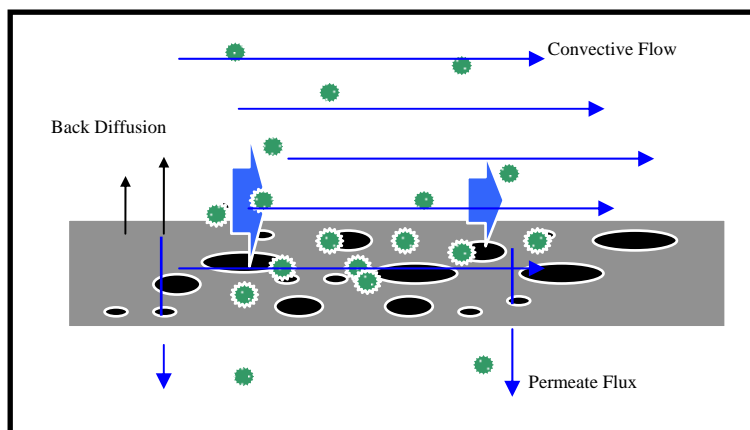


Figure II.1 Solute Transport Across a Membrane

In the hereby-intended investigation, the advantage of chemically resistant membranes, such as ceramic ones, is that severe cleaning agents, such as diluted caustic solution in combination with sodium hypochloride solutions, may be used to restore the membrane's permeability. However, even with periodic cleaning, the flux cannot always be restored to its initial value.

A study performed at Lund University in Sweden (Jönsson, 1995), showed that it is possible to distinguish between the two flux-reducing phenomena, concentration polarization and fouling. Furthermore, he showed how fouling caused by solute-solute interactions at the surface of the membrane and solute-membrane interactions in the membrane matrix may be distinguished. The study was accomplished using a turbulence-promoting module in order to determine the reversibility of the flux reduction in both hydrophobic and hydrophilic membranes, with minimal effects on trans-membrane pressure. Jönsson observed that during the ultrafiltration of silica solutions, permeate flux varied proportional to the solution's shear rate up to a maximum permeate flux, and that it was reversible upon shear rate reduction. This phenomenon was

attributed to accumulation of material in the boundary layer or concentration polarization. On the other hand, upon addition of sodium chloride to the solutions, a different flux behavior was observed. In this case, flux did not vary with increasing shear rate, attributed to deposition of silica aggregates promoted by the decrease in particle electrostatic repulsion caused by the ionic influence of sodium chloride. Finally, it was determined that solute deposition on the membrane matrix, causing blockage of pores and therefore diminishing flux, can be detected when flux does not vary with shear rate at various concentrations, even when the membrane/solute chemical characteristics, such as its hydrophilic or hydrophobic tendency are switched.

In another investigation (Elzo, et. al., 1996), researches attempted to analyze the factors leading to the retention of particles on a cellulose diacetate model membrane, which eventually lead to surface fouling. This group of researchers used a hydrodynamic method in which the release of deposited particles was measured under the action of fluid flow. This approach was based on a particle torque balance, resulting in the quantification of the net adhesive forces acting on the particles bonded on a plane surface under the action of a shear flow. The investigators were particularly interested in the factors leading to the fouling of organic membranes used for drinking water production. Several other factors were studied such as pH, solution salinity, and the effects of adsorbed polymers and non-ionic surfactants on the particles. In general, their results showed that a higher hydrodynamic force is needed to release particles from the surface when either the pH was acidic or the ionic strength of the solution was increased. These two factors are correlated to minimizing the electrostatic repulsive force barrier among

particles, therefore enhancing the effects of the Van der Waals attractive energy among particles, results in increased net adhesive forces both among particles and between particles and membrane surfaces. Such adhesive force quantification can aid to determine which factors are more influential in particle removal from membrane surfaces.

#### F. Mathematical models review

One of the most basic and general model for filtration is that based on the well known Darcy's law modified to include the contribution of the boundary layer resistance or  $R_{bl}$ , resulting in

$$J_v = \frac{P_{TM}}{\eta_0 \cdot (R_m + R_{bl})} \quad (1)$$

where,  $P_{TM}$  is the transmembrane pressure,  $\eta_0$  is the solution viscosity and  $R_m$  is the membrane resistance. This model incorporates the resistance of both the membrane and that of a layer of solutes working in series with one another to obstruct the free path of permeate. Deposition of solutes on the membrane surface is a well-known phenomena that may occur even at low concentrations (Van Den Berg, et. al., 1990) and will decrease the permeate flux rate as observed in our experimental results.

Various approaches can be taken in trying to describe this concentration polarization phenomena, or build-up of solute near the membrane interface. The first and most basic approach is the "Cake-Filtration" expressed in the following equation

$$C_b \cdot R_{obs} \cdot V_p = \delta \cdot A \cdot C_{bl} \quad (2)$$

which assumes a constant concentration in the layer near the membrane of area  $A$ , dependent of applied pressure and increases in thickness with increasing permeate volume. The major constraint of this method typically is the to determine experimentally either the boundary layer concentration ( $C_{bl}$ ) or its thickness ( $\delta$ ), in order to be able complete the mass balance across the membrane where  $R_{obs}$  is the observed retention defined by  $1 - C_p/C_b$ ,  $A$  is the membrane area,  $C_p$  is the permeate concentration and  $C_b$  is the bulk or the feed concentration. Typically the only constraint for the usage of this model would be a relationship to determine  $C_{bl}$  directly from experimental data.

Defining the boundary layer resistance  $R_{bl}$  as its thickness  $\delta$  times the specific resistance  $r_{bl}$  of the boundary layer, and using the hydrodynamic model of resistances, one can derive a flux relationship as a function of permeate volume ( $V_p$ ) at constant  $P_{TM}$ . This relationship is given by

$$\frac{1}{J_v} = \frac{1}{J_w} + \left( \frac{\eta_0 C_b R_{obs}}{P_{TM}} \right) \cdot \left( \frac{r_{bl}}{C_{bl}} \right) \cdot \left( \frac{V_p}{A} \right) \quad (3)$$

Integrating Equation (3) from the flux definition equal to  $dV_p/Adt$ , the resulting expression is

$$t = \left( \frac{\eta_0 C_b R_{obs}}{P_{TM}} \right) \cdot \left( \frac{r_{bl}}{C_{bl}} \right) \cdot \left( \frac{V_p}{A} \right)^2 \quad (4)$$

which is the well known relationship for dead end filtration, where the solvent flux  $J_v \sim 1/t^{0.5}$  or  $V_p \sim t^{0.5}$ . To determine the specific resistance of the boundary layer ( $r_{bl}$ ), various

models such as the filtration model and the boundary layer resistance model are well documented. For instance, the filtration model uses the Kozeny-Carman relationship

$$r_{bl} = 180 \cdot \frac{(1 - \varepsilon)^2}{[(d_s)^2 \varepsilon^3]} \quad (5)$$

where  $\varepsilon$  is the porosity of the concentrated layer and  $d_s$  is the “diameter” of the solute particle.

The “boundary layer resistance model” describes the specific resistance with the relationship

$$\frac{1}{r_{bl}} = \frac{\eta_0 s(C)}{C(1 - \nu_1 / \nu_0)} \quad (6)$$

where  $C$  is the concentration of the concentrated layer,  $s(C)$  is the sedimentation coefficient at  $C$  and  $\nu_1, \nu_0$  are the partial specific volumes of the solute and the solvent respectively. The model is based on the correspondence of the permeability (inverse  $r_{bl}$ ) of a concentrated layer for the solvent near a membrane interface and the permeability of a solute in a stagnant solution, as occurring during a sedimentation experiment.

An alternative model is that of the “film theory”. From a mass balance around a film on the membrane using the change in concentration with time at the film equals the convective transport toward the membrane minus the back diffusion from the film as a result of the concentration gradient, emerges the relationship

$$\frac{\partial C}{\partial t} + J_v \frac{\partial C}{\partial x} = \partial \left( D \cdot \frac{\partial C}{\partial x} \right) / \partial x \quad (7)$$

Assuming a constant diffusion coefficient and steady state conditions, the “simplified film theory” relationship results in

$$J_v = \left( \frac{D}{\delta} \right) \ln \left\{ \frac{C_{(\delta-x)} - C_p}{C_b - C_p} \right\} \quad (8)$$

where  $D/\delta$  is the mass transfer coefficient,  $C_b$  is the bulk concentration and  $C_{(\delta-x)}$  is the concentration across the film thickness.  $D/\delta$  and  $C_{(\delta-x)}$  are equipment and solute dependent.

The “Osmotic Pressure Model” general concept is that a macromolecular solution has a very small osmotic pressure in comparison to an equal weight-percentage low molecular salt solution. Given that a large concentration can build-up during filtration, the osmotic pressure at the membrane surface can increase enormously. For ideal diluted solutions, this osmotic pressure can be calculated from the van’t Hoff equation for non-electrolytic and dilute solutions

$$\pi = R \cdot T \cdot \frac{C_s}{M_s} \quad (9)$$

where  $R$  is the gas constant,  $C_s$  stands for solute concentration,  $T$  is the absolute temperature and  $M_s$  the solute molecular weight. This coefficient would represent the osmotic pressure of the solution, that is, the baseline from which the osmotic pressure would increase near the membrane as the concentration builds up due to polarization.

On the same basis, this concentration build up at the membrane would give place to an additional component of resistance due to polarization. Therefore, taking into account

the osmotic pressure and the polarization resistance, Equation (1) can be rewritten in the form

$$J_v = \left( \frac{P_{TM} - \sigma \cdot \Delta\pi}{\eta_0 (R_m + R_{bl})} \right) \quad (10)$$

where  $\sigma$  is the rejection coefficient and  $\eta_0$  is the viscosity of the solvent in Pa-s. The term  $\Delta\pi$  is the osmotic pressure across the membrane, which in our case study becomes  $\pi_m$ , the osmotic pressure at the membrane. This assumption is made on the basis that for dilute solutions of macromolecules the osmotic pressure is negligible, that is, there is no contribution from the bulk nor the permeate to the osmotic pressure magnitude. The term  $\pi_m$  originates from the concentration generated from the polarization effect close to the membrane.

Notice that the osmotic term is subtracted from the hydraulic pressure term given that the driving force originating from the osmotic pressure is in the opposite direction to that of the hydraulic pressure. For a full rejection system the coefficient  $\sigma$  equals one. Then, Equation (10) can be re-written in the form of

$$J_v = \left( \frac{P_{TM} - \pi_m}{\eta_0 (R_m + R_{bl})} \right) \quad (11)$$

Scrutinizing Equation (8) somewhat further can lead to the assumption that from a semi-logarithmic plot of  $J_v$  versus  $\ln(C_b)$ , the extrapolation to zero flux can result in a membrane concentration corresponding to the osmotic pressure, which is equal to the

applied  $P_{TM}$ . This could be another way of estimating  $\pi_m$ . This approach assumes that a membrane concentration is to be reached at the membrane interface being it a function of  $P_{TM}$ . Furthermore, assuming  $\pi_m = a \cdot C^n$  to be a functional relationship with concentration (Bakjer et. al., 1985) and combining it with Equation (11) the resulting relationship is

$$J_v = \frac{[P_{TM} - a \cdot C_b^n \cdot \exp(nJ_v/k)]}{\eta_0 R_m} \quad (12)$$

From the partial derivative with  $\ln(C_b)$ , the relationship predicts that for high osmotic pressures, the value for the mass transfer coefficient  $k$  can be estimated as for the

$J_v$

versus  $\ln(C_b)$  plots of the simplified film model.

### **III. MATERIALS AND PROCEDURES**

The materials and procedures used in this investigation will be presented in three sections, namely, (A) Batch mode ultrafiltration, (B) Endotoxins and Limulus Amebocyte Lysate (LAL) assay and (C) Cleaning and Sterilization in Place.

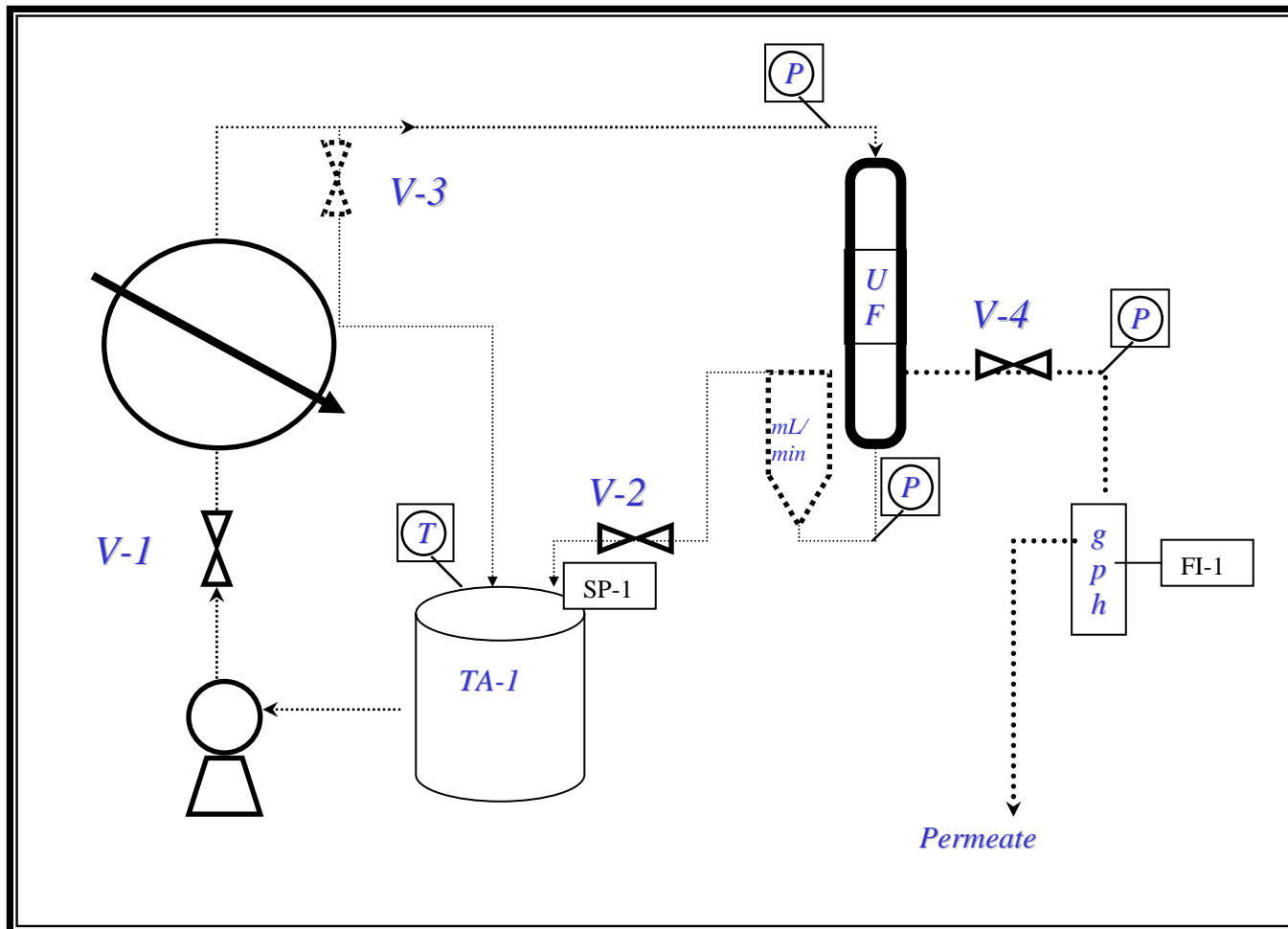
#### **A. Batch mode ultrafiltration**

The ultrafiltration system utilized in this research was the bench top pilot unit by U.S. Filter Co. model 1T1, photographed in Figure III.1. The system's material of construction was stainless steel in all its wetted parts, with piping of 0.5 inches inside diameter, ending in sanitary flanges, interconnected with triclover wraps. Pressure was mainly controlled with diaphragm valve V-1, while V-2 did the analogous for flow rate (refer to Figure III.2). In addition, needle valve V-3 was used to control the recycle rate while needle valve V-4 was used to control the transmembrane pressure together with V-1. The system's reservoir, TA-1, was equipped with a full jacket, which in conjunction with heat exchanger HE-1, provided the heat exchange surface area for the recycling coolant. Centrifugal pump PU-1 worked with 115 AC voltage, and provided an average power of 0.5 Hp.



Figure III.1 Bench-top Pilot Unit (by U.S.Filter Co.)

Figure III.2 Flow Diagram of Experimental System



Some ancillary equipment and general utilities were added to the pilot unit as described in Table III.1.

<b>Ancillary Equipment</b>	<b>Functionality</b>
Thermocouple	Used to monitor temperature at water reservoir
Flowmeter (mL/min)	Monitored concentrate flow rate
Flowmeter (gph)	Monitor permeate flow rate
Cooling Bath	Recirculation and tempering of coolant
Nitrogen filter	Dehumidified and removed extraneous matter from nitrogen

Table III.1 Ancillary equipment to USFilter's 1T1 bench top pilot unit.

Selection of the filtering membrane was based on observations from previous research discussed in the Literature Review section, which sustained that membranes with nominal molecular weight cut-off (NMWCO) of 5,000 to 10,000 retain lipopolysaccharides to concentrations below 0.03 EU/mL. The ceramic membrane selected was the USFilter's single tube element with the characteristics tabulated in Table III.2.

Water used in all the experimental runs was assayed to have less than 0.03 EU/mL and was obtained from a Millipore laboratory scale system. This system was supplied with potable water, which was processed across an activated carbon filter, a reverse osmosis membrane, ultraviolet treatment and finally through a 0.2 micron filter. The resistivity of the experimental water was constantly monitored to be 18.2 Ohms, in agreement with literature data for pure water free of solutes and ions. In general, water was collected into a sterilized 8 L container and then transfer into TA-1 by pressurizing

the container and allowing pressure relief by displacing volume outside via subsurface line.

<i>Ceramic element parameters</i>	<i>Max</i>	<i>Min</i>
Membrane Surface Area, m <sup>2</sup>	0.0055	NA
Membrane Inner Diameter, m	0.007	NA
Membrane Outer Diameter, m	0.01	NA
Membrane Length, m	0.25	NA
Design Pressure, Kpa	NA	
Membrane	792.90	NA
System	482.63	NA
Design Temperature, °C	NA	
Membrane	225	NA
System	100	NA
Permeate Range, m <sup>3</sup> /s	0.009	0.0003
L/s	9	0.3

Table III.2 Ultrafiltration element characteristics.

In general, the experimental procedure was to charge 2 liters of endotoxin-free water, that is, with less than 0.03 EU/mL as per LAL assay, into TA-1 followed by the dilution of the corresponding concentration of endotoxins. The batch was recirculated for 5 minutes in order to homogenize its content and temperature. The temperature range at which all trials were performed was 25-30°C, controlled by the automated cooling bath recirculating ethylene glycol through the system's jackets. At all times the permeate stream was recycled back to TA-1 in order to maintain a constant endotoxin concentration.

Valves V-1 and V-2 were graduated to establish a maximum inlet pressure ( $P_{In}$ ) for the desired system flow rate. At this point, samples of the feed, the concentrate and the permeate were collected into 10 mL pyrogen-free vials. Varying needle valve V-4

controlled transmembrane pressure ( $P_{TM}$ ). Permeate flow was recorded from FI-1 in intervals of  $P_{TM}$  equal to 5 psig. Readings were collected as allowed by the full opening of V-3, at which point  $P_{TM}$  was the maximum for the particular system flow rate.

Once the permeate flow readings were recorded, additional samples of the feed, concentrate and the permeate were collected. The endotoxin content of these samples would be compared to that of those taken at the beginning of the corresponding batch run. Any difference would have been considered as retained by the system. The samples were stored in a laboratory refrigerator, in order to avoid microbial growth in the samples, and assayed for endotoxins within a period of 24 hours. Specifically, the feed samples were collected from TA-1 using pyrogen free pipettes, the concentrate samples via sampling port (SP-1), while the permeate sample was collected from the permeate recycle line. SP-1 was always drained about 50 mL prior to the collection of the actual sample. This batch procedure was used for various feed concentrations and system flow rates. The approach followed was that of a  $3^2$  factorial design of experiment. The two factors or independent variables were feed concentration and feed rate. Each was studied at three levels.

For the feed concentrations the levels were 100, 500 and 667 EU/mL. There exist various ideas on which is the proper way to challenge the endotoxin retention of water depyrogenizing UF systems. Among those, it is proposed that standard, commercially available endotoxin be added to the solution to test for both worst-case and failure limits. On the other hand, it is suggested that normal in-plant bacterial flora should be used to generate a pyrogen load in the product, and finally, other experts argue against adding

any pyrogens beyond the amount that normally occurs in the process Novitsky, 1994). Nonetheless, the general objective of this work was to assess the interaction of operational parameters with endotoxin retention over a wide range of concentrations. It was perceived, that most viable way to accomplish this was by artificially providing endotoxin concentrations from commercially available sources.

The concentrations used were considerably higher (in the order of magnitude of  $10^2$  to  $10^3$ ) than feed streams of a depyrogenation system in a pharmaceutical setting. The justification for such a selection was based on the intent of simulating concentration polarization scenarios, as well as on the intent of maximizing the probabilities of lypopolysaccharide molecules challenging the retentiveness of the ultrafiltration membrane.

Similarly, the system flow rates corresponded to Reynolds numbers of laminar, transition and turbulent. The original unit pilot system did not provide for flows below the transition region, therefore inhibiting the accomplishment of experiments at the laminar flow region. By adding the recycle leg of the pump exhaust back to the reservoir allowed for slower linear flows across the same cross sectional area at the annular ceramic membrane, resulting in flow profiles below the transition Reynolds.

In order to generate a database, which would serve as a baseline for the pilot plant's performance, pure water trials were done on the experimental ceramic membrane. These trials were done across the entire pressure and flow experimental profile of the system, at a temperature between 25 and 30°C. By comparing the pure water flux results with

manufacturer data, it could be determined if membrane usage, cleaning and, handling could have compromised the integrity of the membranes.

### **B. Endotoxins and Limulus Amebocyte Lysate (LAL) assay**

The endotoxins diluted into TA-1 were purchased dehydrated in various endotoxin vial counts, to be referred hereon as Control Standard Endotoxin (C.S.E.). Each vial could be traced back to a manufacturing lot number. The C.S.E. were reconstituted from their lyophilized state by adding LAL Reagent Water (L.R.W.), followed by mixing using a vortex agitator for 30 minutes. Depending on the desired feed concentration, the corresponding volume was pipetted out of the C.S.E. solution and diluted into TA-1.

With regards to the LAL in-vitro assay, the reagents included the reagent Limulus Amebocyte Lysate of 0.03 EU/mL sensitivity and Reference Standard Endotoxin (R.S.E.). LAL is an extract made from the blood cells (amebocytes) of the horseshoe crab. During the 1960's, Bang and Levin (Novitsky, 1994) discovered that the extract, compound of a pre-clotting enzyme (zymogen), a clotting protein (coagulogen) and inorganic salts, reacted to the presence of minute amounts of endotoxins.

Laboratory equipment used during the execution of LAL assays and endotoxins hydration included: 17 x 100 mm and 10 x 75 mm depyrogenated test tubes, used for sample dilutions and LAL assaying, 1, 5 and 10 mL serological, disposable and depyrogenated pipettes, depyrogenated micropipette tips and high precision micropipettes. Other miscellaneous materials used in the microbiology lab during LAL assaying included: 1) vibrating vortex agitator to homogenize dilutions, 2) Water bath adjusted to  $37 \pm 1$  °C for LAL vials aging, 3) L.P.H. germicide, 4) propane burner for

superficial and airborne sterilization 4) sterilized polypropylene gloves 5) test tube racks and 6) chronometer.

In general, the assay was performed by adding 0.1 mL of reconstituted 0.03 EU/mL LAL to an equal volume of liquid sample in a 10 x 75 mm test tube. Content was mixed avoiding formation of foam and the mixture was placed in a test tube support and then incubated undisturbed at  $37 \pm 1$  °C for  $60 \pm 2$  minutes. C.S.E. diluted to a known concentration and L.R.W. were used as the positive and negative controls respectively for the LAL assay. Following incubation the test was scored by inverting the reaction tubes 180 degrees. A positive test (sample with  $> 0.03$  EU/mL) was scored if a solid gel-clot is formed and withstands the inversion. On the other hand, a negative test (sample with  $< 0.03$  EU/mL) was scored if no gel-clot was formed or if the gel-clot broke on inversion.

For the cases where positive results were obtained, the corresponding sample was diluted serially to orders of 50%, that is, the positive sample where diluted to 50%, 25%, 12.5%, etc., in 17 x 100 mm test tubes. Following the same methodology for LAL assaying described previously; testing was repeated until a dilution producing a negative result was obtained. Each dilution was tested in duplicate. Since the dilution percent was decreased as long as a positive assay was obtained, the ultimate result was a final positive dilution followed by a final negative dilution. These determined respectively the upper and lower limits of the endotoxin concentration range in the initially undiluted positive sample.

In order to numerically assess the sensitivity of the LAL vials, prior to usage, known endotoxin concentrations were tested with the particular LAL vial in quadruplicates. In

principle, a 5000 EU vial was reconstituted with 5 mL of L.P.W., a sample of which was diluted serially to specific concentrations. These concentrations were represented by multiples of the value lambda ( $\lambda$ ). The ratio of the specific concentration and the sensitivity of the L.A.L determine these multiples, that is,

$$\lambda = (\text{concentration in EU/mL}) / (\text{sensitivity of LAL in EU/mL}).$$

For example, a sample with an  $8\lambda$  value corresponds to a 0.25 EU/mL concentration if analyzed with a L.A.L of 0.03 EU/mL sensitivity.

The replicates analyzed for this sensitivity check corresponded to  $\lambda$  values of 4, 2, 1, 0.5, 0.25, that is, dilutions of 0.125, 0.063, 0.031, 0.016 and 0.008 EU/mL. For each set of  $\lambda$ s the LAL assay was performed and an endpoint concentration determined by the last positive result in the set. The geometric media of these endpoint concentrations was calculated and a negative control tested with the same LAL. The sensitivity of the vial in question was said to be confirmed when the negative control resulted in a negative test and, the geometric media calculated was greater than  $0.5\lambda$  (0.016 EU/mL) and less than  $2\lambda$  (0.063 EU/mL).

Once confirmed the sensitivity of the LAL, the same was ready to be used to detect endotoxins in the different samples collected from the ultrafiltration system. Following the recommendation of the manufacturer, the lysate was stored cold from 2-8 °C and used within 24 hours of its reconstitution.

### **C. Cleaning and Sterilization in Place**

Start-up and operation of the pilot unit involved a sequence of steps that ensured the sterilization of the system and consequently the reliability of the data generated. In the case of ultrafiltration systems, a crucial step is cleaning, which involves effectively removing all the process streams from the system, regenerating the membrane to restore flow rates, sterilizing the membranes and the hardware and effectively removing the cleaning agents. However, none of this is attainable without proper mechanical set up of the system.

Correct installation and assembly of the pilot plant was verified by monitoring leakages during pressure tests. Pressure tests were carried at 10 psig using an inert gas, in this case nitrogen. The acceptance criterion used was lost less than 1.0 psig during a 10 minutes time period. This test was performed prior to all experiments. Once the system was verified to be leakage-free, the standard procedure prior to every experiment was to sterilize and depyrogenize the system. This was the case after every endotoxin challenge since parts of the system were not completely isolated from the environment and, in case there was any dead legs that would harvest microbial growth during shot downs periods.

The sterilization in place (SIP) consisted of flushing the system with a 70% isopropyl alcohol solution. Alcohols denature proteins, possibly by dehydration, and act as solvents for lipids. Thus, membranes are likely to be disrupted and enzymes inactivated in the presence of alcohol, resulting in the chemical killing of microorganisms. Two liters of this solution were circulated across the system at a flow rate of 2 L/min, for 10 minutes keeping a temperature below 50 °C to avoid solution vaporization and a pressure buildup. All permeates were recycled to the storage vessel

for the first 5 minutes, and thereafter collected from permeate ports in order to allow for all sampling valves to be flushed with the sterilizing solution.

After emptying the system of the sterilizing solution, residues were flushed from the system by two -liter flushes of pure water at a flow rate of 2 L/min. Each flush was recirculated for 2 minutes and then transferred out via TA-1 bottom valve. Samples analyzed via High Performance Liquid Chromatography (HPLC) determined that the used flushing routine dropped isopropyl alcohol levels below 100 ppm, which was used as the acceptance criteria.

The SIP was followed by a depyrogenation process, or cleaning in place (CIP). The treatment included flushes of 2 liters of a 2-w/w % NaOH solution. These solution composition were found to be effective in depyrogenating a similar system by Engel and Cheung during a manufacturing scale validation exercise at the Merck & Co. West Point facilities in 1994 (Engel, 1994). They reported 100% trans-membrane pressure restitution after this CIP treatment, when compared to both, data provided by the manufacturer for new membranes as well as for pure water flux vs. pressure data.

The objective of the CIP was to break down the endotoxins (lipopolysacharides) using a strong base (pH ~13.4). The solution was pumped through the system at a 2 L/min in a recycle mode, for 15 minutes, keeping the temperature below 50 °C to avoid solution vaporization. After emptying the system of the cleaning solution, residues were flushed from the system by two-liter flushes of pure water at a flow rate of 2 L/min. Each flush was recirculated for 1 minute and then transferred out via TA-1 bottom valve.

Samples for pH determined that the flushing routine used attained neutral values (pH~7), suggesting NaOH was removed effectively.

Both the SIP and CIP cycles were performed using turbulent flows, therefore using not only the chemical properties of the solutions but also the momentum transfer of the flow to disengage any contaminating agent from the system's surface. Cleaning procedures were rigorously implemented during this investigation. Recent investigations by Lindau et. al. (Lindau, 1995) revealed, that often, the reestablishment of the initial pure water flow (PWF) as the parameter to determine membrane regeneration could be misleading. This was the case during the ultrafiltration of octanoic acid solutions in his investigation. Membrane inspection by means of Fourier Transform Infra Red spectroscopy uncovered the presence of octanoic acid adsorbed in the membrane, even when PWF had been regained after cleaning.

## IV. RESULTS AND DISCUSSION

The results will be presented in two sections namely, (A) Pure water results, and, (B) Constant endotoxin concentration results. Permeate flux data was averaged according to feed rates  $N_{Re}$ , that is, according to laminar ( $N_{Re} < 2100$ ), transition ( $2100 < N_{Re} < 4200$ ) and turbulent ( $N_{Re} > 4200$ ) flow regions. The Reynolds number values are the result of the discrete flow rates measured by the system instrumentation and the tubing geometry all combined in the formula

$$N_{Re} = \frac{\rho \cdot d \cdot v}{\eta}$$

where  $\rho$  stands for water density,  $\eta$  stands for water viscosity,  $d$  stands for flow path diameter and  $v$  stands for linear velocity of the fluid. Hereon on this manuscript, the identification of laminar, transition and turbulent feed rates, will refer to the traditional  $N_{Re}$  ranges.

### A. Pure water results

The results obtained for water with  $< 0.03$  EU/mL (also referred to as “pure water”) are presented in Figure IV.1. The ranges were identified as pertaining to one of the flow regions, namely laminar, transition and turbulent, if any of them applied. They exhibit an evident proportionality with  $P_{TM}$  all throughout the experimental pressure range, that is, from 5 to 50 psig. This range was the span controllable by the system’s instrumentation. Maximum permeate fluxes were obtained at the maximum studied  $P_{TM}$  of 50 psig. Turbulent flow produced an average 18.2% higher permeates fluxes than the transition flow and 18.8% higher than the laminar flow rates.

The linear profile in the probability plot presented in Figure IV.2 shows no evidence of standard error outsiders. Therefore, this graphical verification supports the usage of the standard error as an appropriate normal statistic to describe the error around the averaged fluxes in each flow region at different transmembranic pressures. All the flux data and associated tabulations to calculate the standard errors are included in Appendix 4.

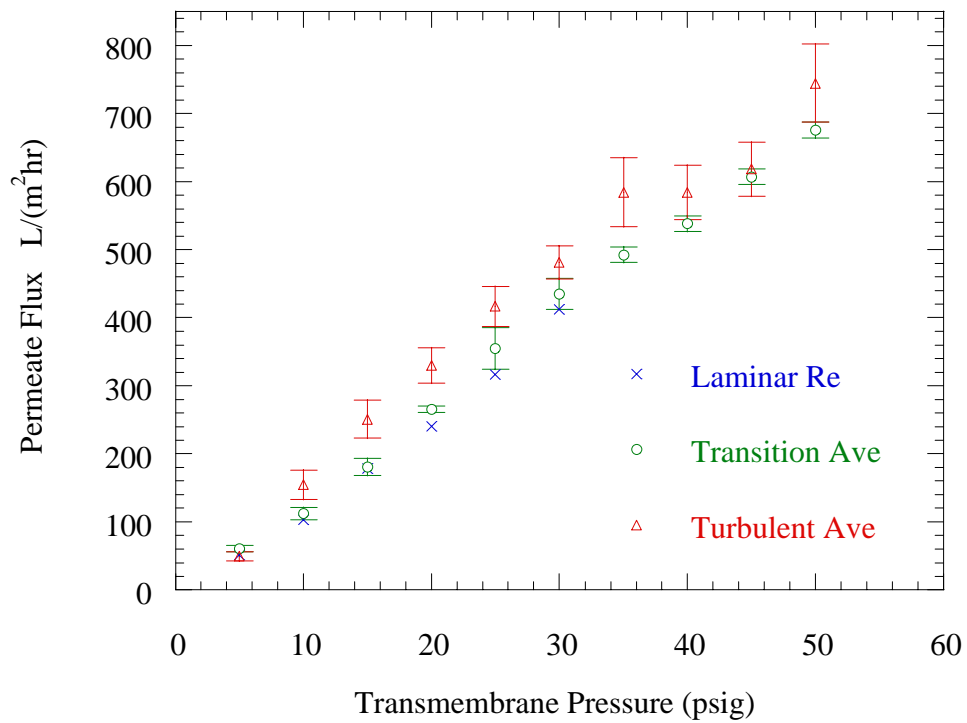


Figure IV.1: Averaged results obtained for water with  $< 0.03$  EU/mL grouped in  $N_{Re}$  regions and enclosed by the corresponding standard error bars.

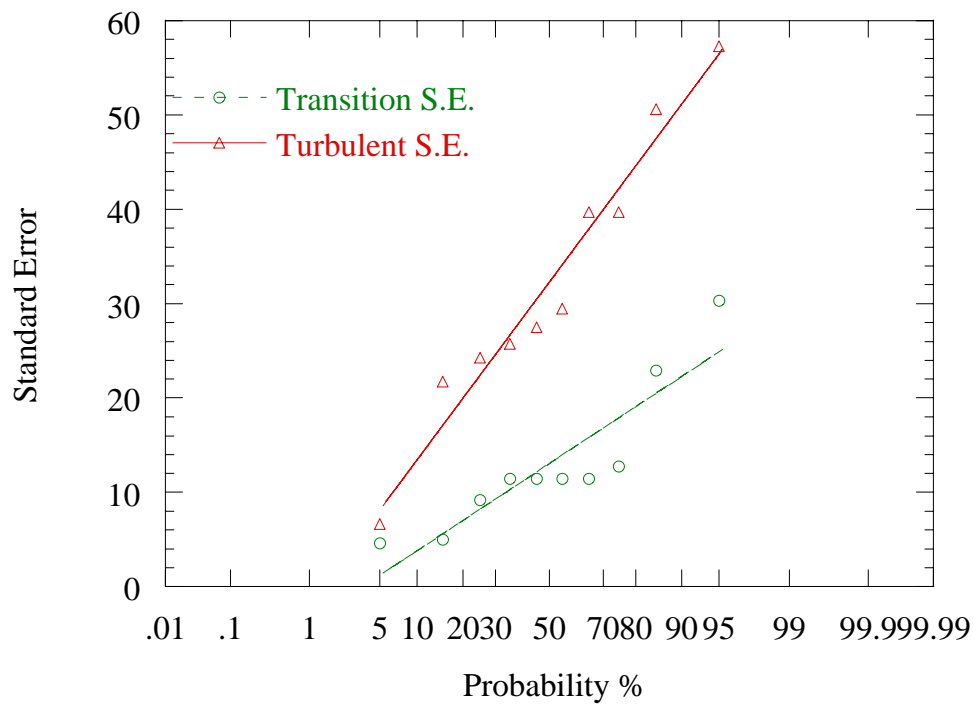


Figure IV.2 Probability plot of standard errors for water with < 0.03 EU/mL, grouped by  $N_{Re}$ .

Utilizing Equation (1) and the data collected for pure water allowed the evaluation of the membrane resistance given  $R_{bl}$  originated from the concentration polarization phenomena due to solutes is not present since there is no endotoxin present during this run. Hence, the value  $R_m$  can be estimated and compared to that provided by the manufacturer. Using the viscosity of water at 27.5°C (experimental setting was maintained between from 25 to 30°C), resistance values were calculated from Equation (1) in at different flow regions (refer to Table IV.1).

<b>Reynolds' Range</b>	<b>Average <math>R_m</math> (1/m)</b>
Laminar	$2.19E+09$
Transition	$2.33E+09$
Turbulent	$1.80E+09$
Literature range (extrapolated to 27.5°C)	$[1.13E+09, 1.39E+09]$

Table IV.1: Calculated Membrane Resistance at Different Flow Regions.

A two-sample T-test performed on the  $R_m$  calculations establishes that there is no significant difference between the average result for the laminar and transition Reynolds' regions, at a 95% confidence level (refer to Appendix 17). On the other hand, the lowest average  $R_m$  was obtained for the turbulent region (refer to Figure IV.3). The values obtained at this region are the closest to the manufacturer range, extrapolated at 27.5°C. There is no conclusive evidence of why the experimental calculation for  $R_m$  was higher than those provided by the manufacturer. However, it should be pointed out that the membrane was not pretreated that would open up blocked pores as often suggested by membrane manufacturers.

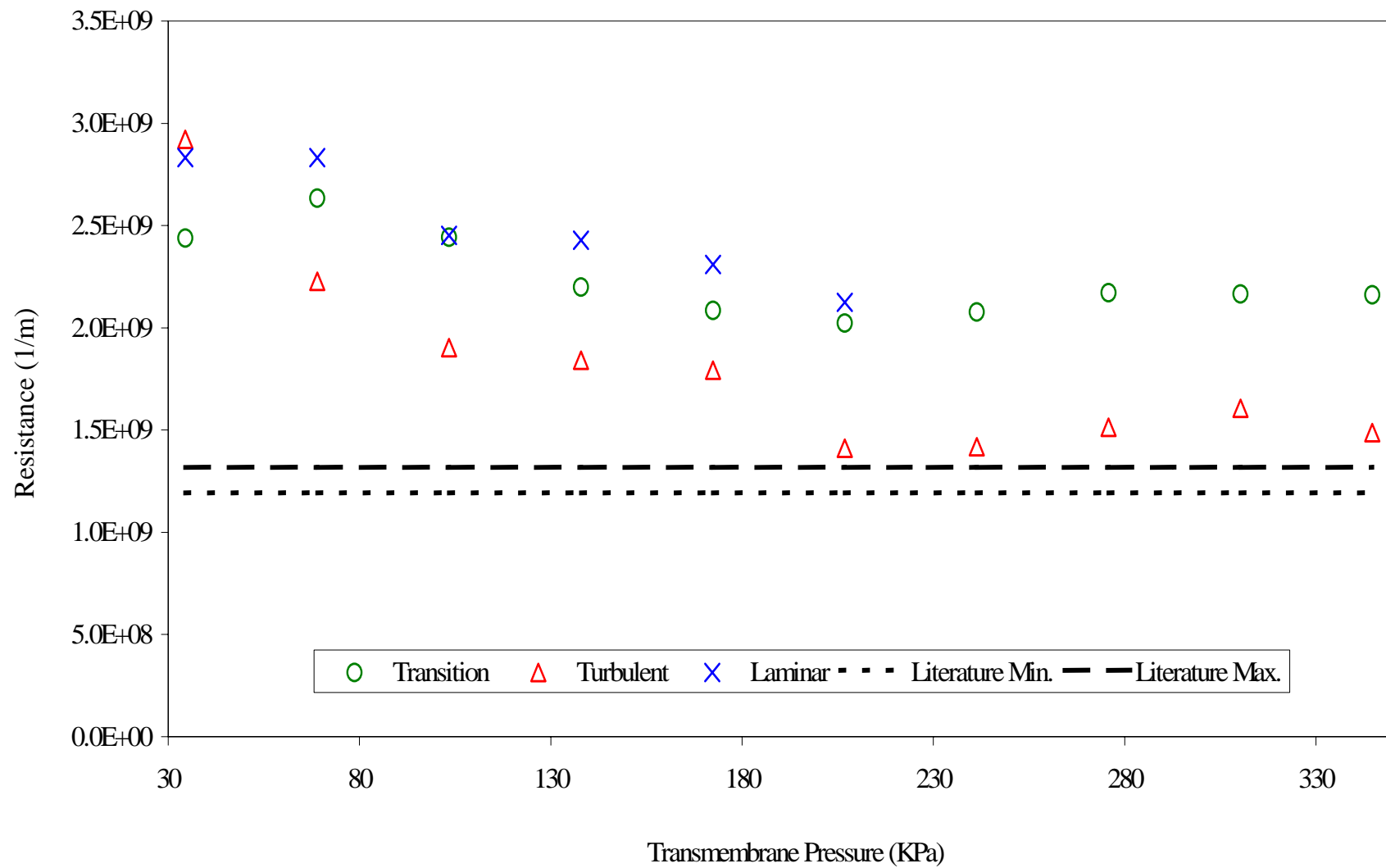


Figure IV.3. Influence of  $P_{TM}$  on the Calculated  $R_m$  Profile.

Another interesting aspect of the calculations for  $R_m$  can be inferred from Figure IV.3. It appears that at low  $P_{TM}$ ,  $R_m$  exhibit higher values. An analysis of variance confirms that  $P_{TM}$  significantly impacts  $R_m$  (refer to Appendix 18). This suggests that the driving potential, namely pressure, may determine the distribution of the flow paths available for transport. This is to say, that this particular ceramic membrane has a pore size distribution rather than an absolute pore size, a fact well known membranes overall.

## **B. Constant endotoxin concentration results**

### **1. 100 EU/mL Feed Concentration**

The proportionality of permeate flux with increasing  $P_{TM}$  was also observed for the feed concentration of 100 EU/mL (refer to Figure IV.4). At this concentration the turbulent flow produced an average 21.2% higher permeate flux than the transition flow. The average difference in permeate flux between turbulent and laminar flows were 21.3% higher than the laminar flow rates.

The linear profile in the probability plot presented in Figure IV.2 shows no clear evidence of standard error outsiders. Therefore, this graphical verification supports the usage of the standard error as an appropriate normal statistic to describe the error around the averaged fluxes in each flow region at different transmembranic pressures. Nonetheless, the standard error obtained for both the turbulent and transition flows at the 50 psig somewhat deviated in magnitude from the rest of the values. These values are observed to drift from the best linear fit in the probability chart. Since the linear fit of the probability distribution is a qualitative test of data, no conclusion can be inferred from these data points. One practical observation is that this phenomenon does occur at other

concentrations but not necessarily at the highest transmembranic pressure, suggesting that reasons associated to the experimental set up might be the cause for such increased standard errors. All the flux data and associated tabulations to calculate the standard errors are included from Appendix 7.

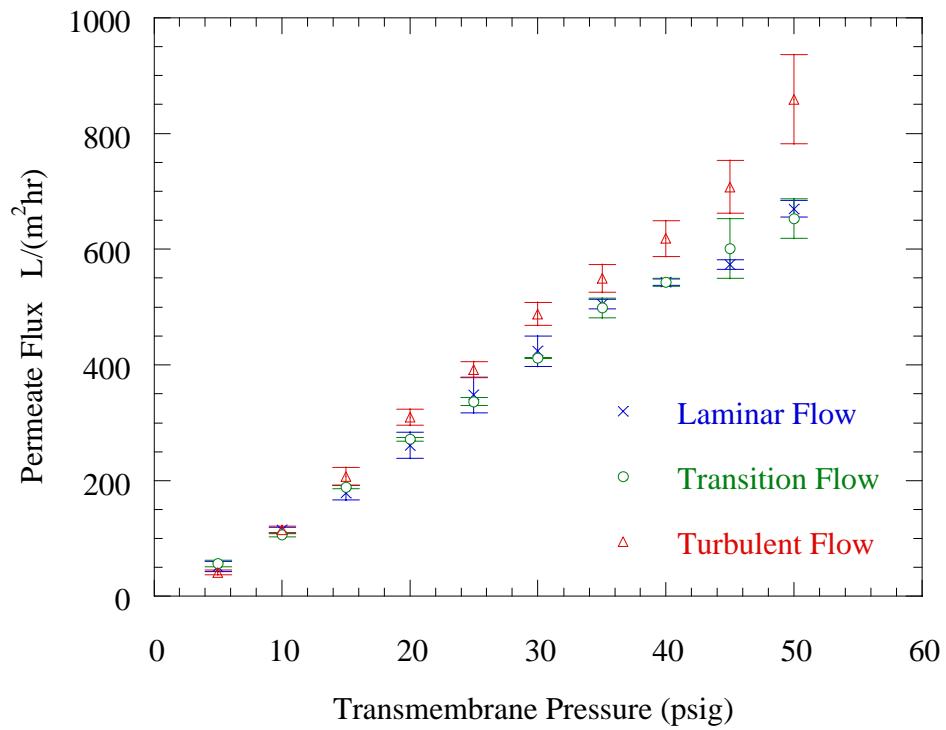


Figure IV.4: Averaged results obtained for water with 100 EU/mL grouped in  $N_{Re}$  regions and enclosed by the corresponding standard error bars.

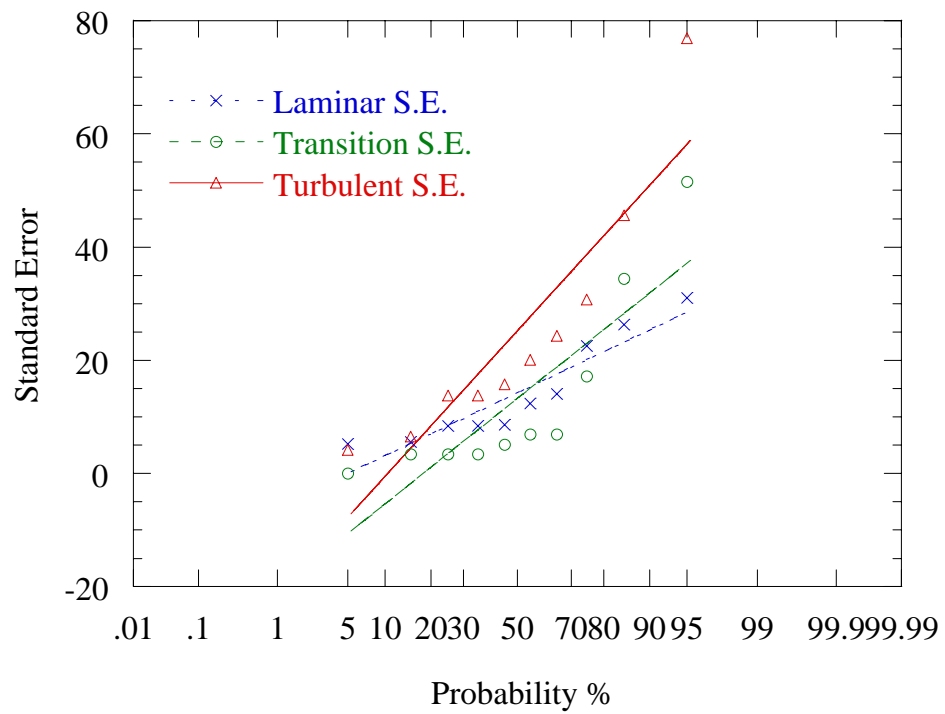


Figure IV.5: Probability plot of standard errors for water with 100 EU/mL, grouped by  $N_{Re}$ .

## 2. 500 EU/mL Endotoxin Concentration

The proportionality of permeate flux with increasing  $P_{TM}$  was also observed for the feed concentration of 500 EU/mL (refer to Figures IV.6). These results were an average 15.6% higher than the transition feed rate results and 11.6% higher than those from the laminar feed rates.

The linear profile in the probability plot presented in Figure IV.7 shows no evidence of standard error outsiders. Therefore, this graphical verification supports the usage of the standard error as an appropriate normal statistic to describe the error around the averaged fluxes in each flow region at different transmembranic pressures. . All the flux data and associated tabulations to calculate the standard errors are included from Appendix 10.

One noticeable detail in Figure IV.7 is the difference in magnitude of standard errors obtained for the transition flow to the rest of the data. No procedure deviation was recorded for this run suggesting validity of the data. It can be argued that the transition flow region is one in which no defined flow pattern exists. That is, the flow velocity profiles are neither parabolic like for laminar regions nor constant, or plug-flow, like for the turbulent flow regions. Theoretically, the large span of fluxes obtained using transition flows could be correlated to lack of predictable flow dynamics using transition flows.

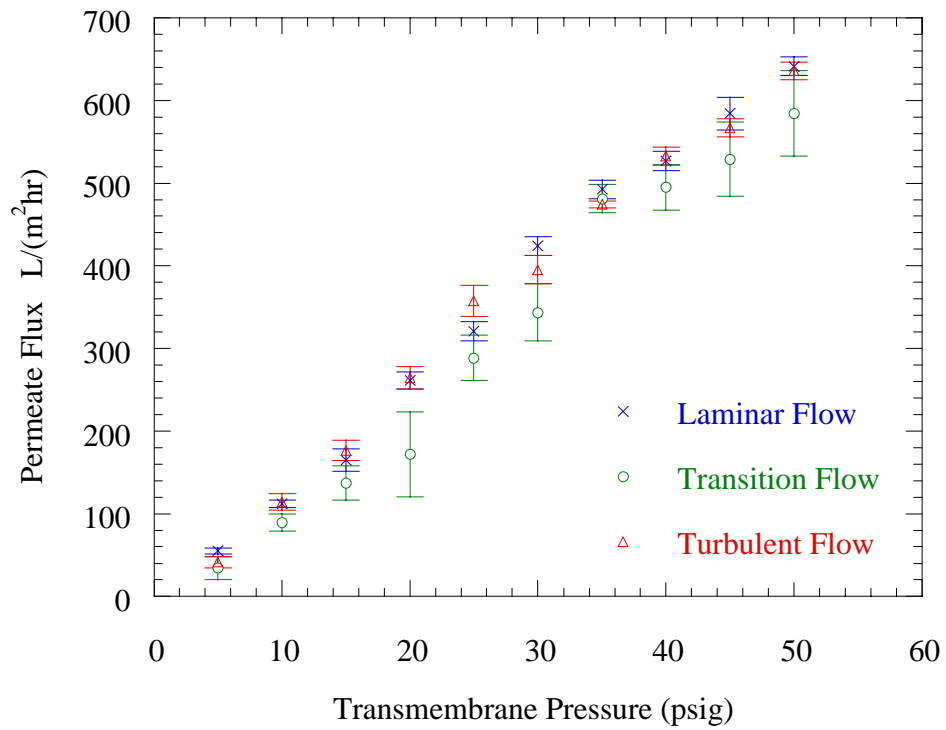


Figure IV.6: Averaged results obtained for water with 500 EU/mL grouped in  $N_{Re}$  regions and enclosed by the corresponding standard error bars.

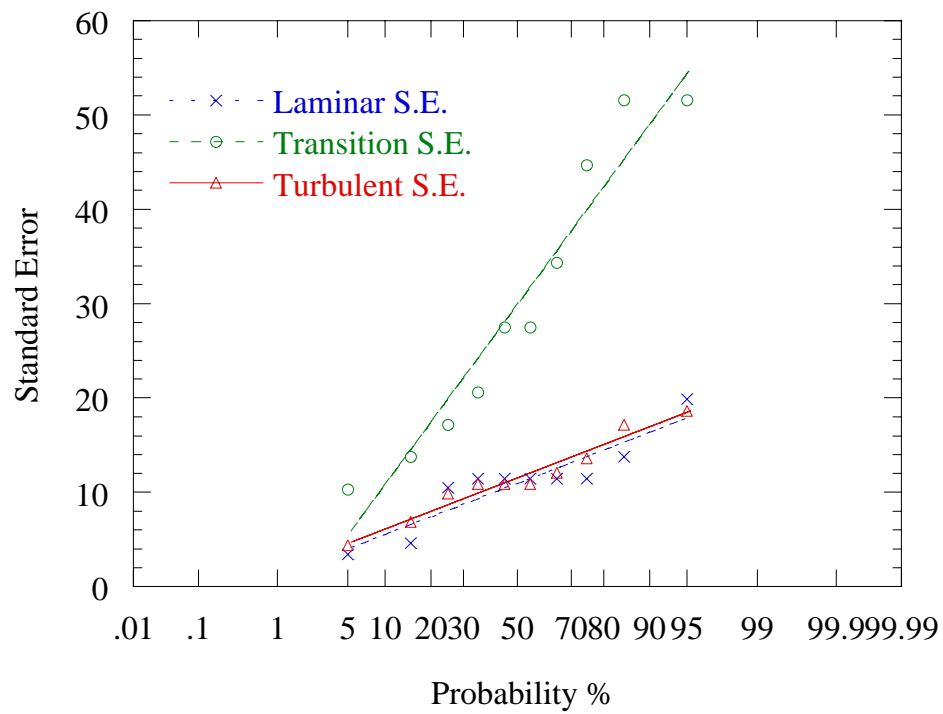


Figure IV.7: Probability plot of standard errors for water with 500 EU/mL, grouped by  $N_{Re}$ .

### 3. 667 EU/mL Endotoxin Concentration

The proportionality of permeate flux with increasing  $P_{TM}$  was also observed for the feed concentration of 667 EU/mL (refer to Figure IV.8). The turbulent feed rate results were an average 46.8% higher than the transition feed rate results and 46.3% higher than those from the laminar feed rates.

The linear profile in the probability plot presented in Figure IV.7 shows evidence of standard error outsiders. Therefore, this graphical verification questions the usage of the standard error as an appropriate normal statistic to describe the error around the averaged fluxes in each flow region at different transmembranic pressures. This observation is expanded on in the following paragraph. All the flux data and associated tabulations to calculate the standard errors are included from Appendix 13.

The permeate flow reading was taken from a float meter of conical diameter. For this particular meter, the scale was not linear across its range, making the reading error to increase proportionally with flow magnitude. The procedure was to allow enough time (approximately 5 minutes) for fluxes to stabilize. However, oscillations were visually detectable around the resulting permeate flow reading. This variation is definitely a component of the standard errors calculated.

A close look at Figures IV.2, 5 and 9 reveals that the magnitude of standard errors was highest for the higher permeate flow readings. In addition, the ranking of overall standard error was highest for turbulent flow runs, followed by transition and laminar flow runs. These observations are valid across all endotoxin concentrations except for

500 EU/mL, where the highest standard error was observed for the transition flow run (refer to Figure IV.7) which was discussed in the previous section.

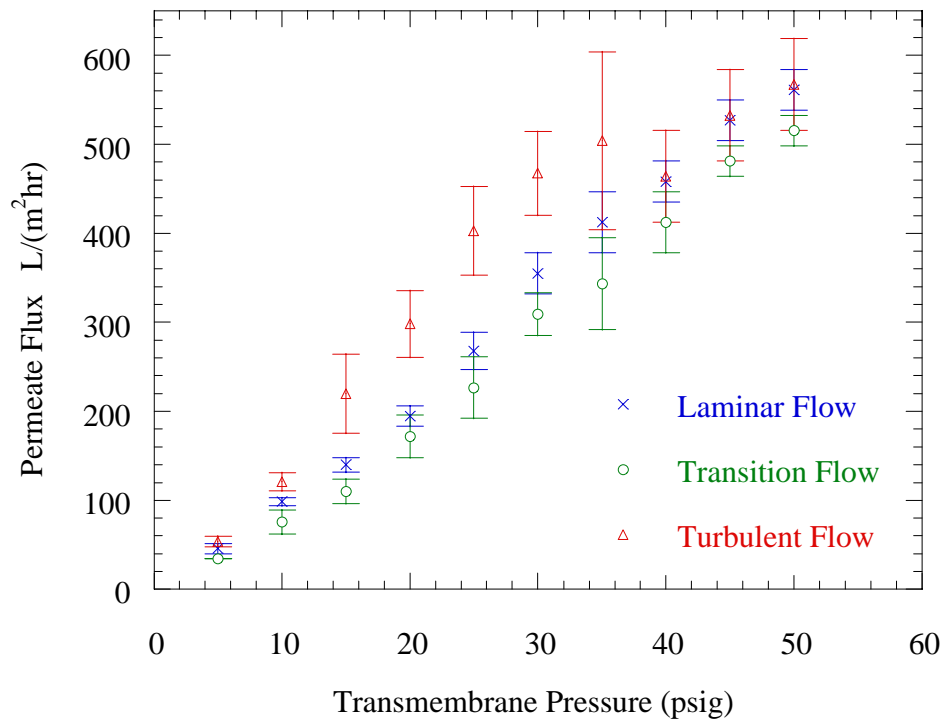


Figure IV.8: Averaged results obtained for water with 667 EU/mL grouped in  $N_{Re}$  regions and enclosed by the corresponding standard error bars.

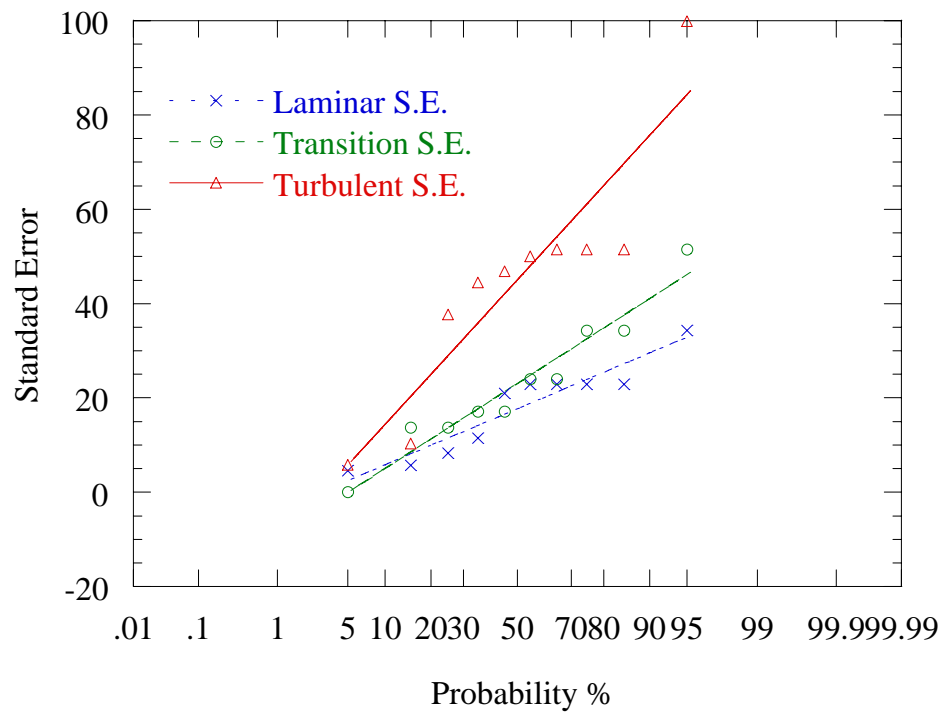


Figure IV.9. Probability plot of standard errors for water with 667 EU/mL, grouped by  $N_{Re}$ .

An overall result of the experimental runs was the pyrogenic reduction obtained at all concentrations and volumetric feed rates. The LAL standard used allowed detection up to 0.03 EU/mL and all assays resulted in negative results at every experimental variation. That is to say, that reductions of 3.52 log, 4.22 log and 4.34 log were obtained for the permeates of the 100, 500 and 667 EU/mL feed concentrations respectively. These values compare satisfactorily to those obtained by Engel and Cheung who in average reported reductions of 5.1 log.

This successful reduction can be attributed to the fact that pyrogens are known to form aggregates in aqueous solutions by exposing their hydrophilic region and engulfing their hydrophobic region forming a micelle-like structures of 0.1  $\mu\text{m}$ . Our subject membrane with a claim cut-off of 200  $\text{\AA}$  could easily reject such particles.

From our experimental results, no endotoxins were detected at any of the experimental conditions making the permeate concentration  $C_p$  equal to 0 (zero), therefore  $R_{obs}$  equal to 1 (one) in the Cake Filtration model in Equation (2). However, a direct relationship does not exist to determine the boundary layer concentration  $C_{bl}$  from experimental data.

Similarly, the hydrodynamic model of resistances in Equation (4), cannot be assessed from our experiments because data of permeate flux was not integrated over time periods, rather was collected as instantaneous values at predetermined settings of feed rate,  $C_b$  and  $P_{TM}$ . Some authors like Howell (Howell et. al. 1980) and Baker (Baker et. al. 1985) have used the Filtration Model in Equation (5) for cross-flow ultrafiltration, however, neither the porosity nor the diameter of solute particles are documented for

endotoxin units in readily available literature nor determined as part of this experimentation. Therefore, the Filtration model is not applicable toward the determination of the boundary layer resistance of this particular case study.

For the “boundary layer resistance model” depicted in Equation (6) a more rigorous experimentation in terms of sedimentation and partial volume determination would have been necessary in order for this model to be used in this investigation. Therefore, neither “boundary layer resistance model” nor the previously discussed “filtration model” are utilized to describe specific resistance for this case study experimental results.

The “gel polarization model” was not used since it assumes that the concentration at the membrane interface cannot exceed a fixed  $C_g$  value. This would cause that an increase of the applied pressure would only result in an increase thickness of the gel layer but not in an increase in flux. During our experimentation, such a limiting pressure was not reached. Consequently, flux was observed to always increase with increasing pressure up to the maximum used of 50 psig. Perhaps, the time per experimental run did not allowed endotoxin to reach  $C_g$  for the concentration range studied.

Nonetheless, for cross-flow filtration the film equation is completed with the experimental observation that full retention of endotoxin was achieved making  $C_p$  equal to zero, resulting in a simplification of Equation (12) for  $J_v$  as follows

$$J_v = (k) \ln \left( \frac{C_m}{C_b} \right) \quad (13)$$

It becomes very difficult from experimentation to determine the mass transfer coefficient  $k$  (or  $D/\delta$ ). However, an estimate can be calculated if the membrane concentration  $C_m$

can be calculated accurately from osmotic pressure data. For this the Osmotic Pressure model will be used.

In order to estimate the osmotic pressure the model used was the Osmotic Pressure models described in Equation (10). From the flux vs.  $P_{TM}$  plots presented earlier at various concentrations, the pressure corresponding to flux equals zero can be extrapolated. A linear regression was calculated using the averaged results at every  $P_{TM}$ , and the resulting equations used to back calculate the pressures at flux equal zero. This pressure corresponds to the equilibrium state at which no transport occurs across the membrane or when  $P_{TM}$  equals  $\pi_m$ . This estimate for  $\pi_m$  has been calculated and the results are presented in Table IV.2.

Feed Reynolds' Range	Estimated $\pi_m$ (kPa)		
	100 EU/mL	500 EU/mL	667 EU/mL
<i>Laminar-Transition</i>	10.8	17.6	19.5
<i>Turbulent</i>	26.7	6.6	16.9

Table IV.2: Estimated Osmotic Pressure at Various Bulk Concentrations

A quick observation of the table shows that the estimated  $\pi_m$  increases with concentration for the laminar-transition results as expected from Equation (9), something that is not observed for the “Turbulent” row. In addition, a row comparison within the same concentration suggests that the estimated  $\pi_m$ . This does not correlate with the empiric assumption that the osmotic pressure is a property of solution and a function of concentration. However, the phenomena of concentration polarization can help explain this apparent contradiction.

The mass transport of endotoxin molecules towards the membrane creates a build up of concentration near the membrane surface. This build-up concentration is not constant between laminar, transition and turbulent flow dynamics simply because the convective component of mass transport away from the membrane is different among them. In theory, a greater flow would pull more molecules away of the membrane and into the main stream. This suggests, that although  $\pi_m$  is a function of concentration, the concentration governing the property may vary due to physical variations of the flow dynamics. This is to say, that while it is expected that increasing concentration would increase osmotic pressure, the hydrodynamic factor counteract this effect by removing accumulated molecules from the boundary layer, making it thinner and less of a resistance and less concentrated. If analyze from a statistical perspective, the experimental results uncover an interaction between the factors feed flow and endotoxin concentration for a resulting permeate flux.

Current literature does not provide estimates of osmotic pressure for pyrogenic aqueous solutions, not allowing comparison with our estimates. Since only estimates of osmotic pressure and a qualitative relationship was established with bulk concentration of endotoxins, no attempt has been made in this manuscript to calculate neither the membrane concentration from Equation (9) nor the mass transfer coefficient from Equation (8).

### **C. Statistical Analysis**

Typically computer models made it possible to analyze the flux response varying only concentration and determining sedimentation coefficients, however, in practice more

than only the selected parameter changes because of mutual relationships. This is when statistical analysis become useful given that multiple parameters, in this case  $P_{TM}$ , feed rate Reynolds and endotoxin concentration can be studied in terms of their effect on flux magnitude. For this purpose, the results for permeate flux were statistically analyzed via analysis of variance (ANOVA) at transmembrane pressures of 5, 25 and 50 psig. Tabulation of the data is presented in Appendices 24 to 33. The two-factor ANOVA's were executed using built-in routines in software Excel®.

Results for  $P_{TM}$  equal to 5 psig are tabulated in Appendix 23. Two ANOVA's were performed, of which one included the turbulent feed rate results. Since the experimental set-up for turbulent flow at this pressure was not replicated, the ANOVA was analyzed without replication. The last ANOVA did not include the turbulent feed rate but included replicates of the experimental set-ups for laminar and transition volumetric feed rates. At the low transmembrane pressure region of 5 psig, the ANOVA results identified the volumetric feed rate and the interaction factor volumetric feed rate-endotoxin concentration as significant factors having an effect in the resulting permeate flux. Endotoxin concentration by itself did not show a significant effect on permeate flux.

Results for  $P_{TM}$  equal to 25 psig are tabulated in Appendix 27. Two ANOVA's were performed, of which one included the turbulent feed rate results. Since the experimental set-up for turbulent flow at this pressure was not replicated, the ANOVA was analyzed without replication. The last ANOVA did not include the turbulent feed rate but included replicates of the experimental set-ups for laminar and transition volumetric feed rates. At the mid transmembrane pressure region of 25 psig, the ANOVA results identified the

endotoxin concentration as a significant factor having an effect in the resulting permeate flux. Volumetric feed rate and the interaction factor volumetric feed rate-endotoxin concentration did not show significant effects on permeate flux.

Results for  $P_{TM}$  equal to 50 psig are tabulated in Appendix 29. One ANOVA was performed that did not include the turbulent feed rate range, but included replicates of the experimental set-ups for laminar and transition volumetric feed rates. At the high transmembrane pressure region of 50 psig, the ANOVA results again identified the endotoxin concentration as a significant factor having an effect in the resulting permeate flux. The dropping effect of the volumetric feed rate and the interaction factor volumetric feed rate-endotoxin concentration on permeate flux was verified at the highest  $P_{TM}$ .

These results suggest that at  $P_{TM}$  higher than 25 psig, the transport mechanism across the ceramic membrane incorporates additional resistances, which theoretically can be attributed to the build up of endotoxins due to concentration polarization. That is, the mechanical forces driving molecules toward the membrane surface overcomes the back diffusion of molecules into the main stream, resulting in a net concentration near the membrane surface. This phenomenon is confirmed at  $P_{TM}$  equal to 50 psig. Furthermore, from the tabulated data it can be seen that the permeate flux also decreases with increasing endotoxin concentration at a constant  $P_{TM}$ .

## V. CONCLUSION

The usage of the U.S. Filters' ZrO<sub>2</sub> on  $\alpha$ -Al<sub>2</sub>O<sub>3</sub> single tube element with NMWCO of 5,000 to 10,000 proved to retain lypopolysaccharides to concentrations below 0.03 EU/mL at a variety of operational conditions. The experimental design approach used allowed the assessment of volumetric feed rates from laminar to turbulent regions based on traditional Reynolds number ranges. In addition, the experimental system set-up allowed for discretely varying transmembrane pressure across typical ultrafiltration ranges.

Linear regression analysis revealed that there is a statistical equivalency between permeates fluxes obtained for the laminar and transition volumetric feed rate experiments. Nonetheless, when the data was grouped in low, medium and high transmembrane pressures, statistical evidence showed that permeate flux variance was a proportional result of other factors such as endotoxin concentration. The general observation was that with increasing transmembrane pressure the main factor dictating ultrafiltration performance was endotoxin concentration. The significance of the volumetric feed rate dropped as a factor when compared to endotoxin concentration when seen from the perspective of increasing transmembrane pressure. It is worth mentioning that this conclusion is limited to the experimental concentrations studied.

The LAL assay used provided a visual indication of the presence of endotoxins on the permeate streams. However, the assay proved to be a technique susceptible to mishandling due to multiple dilutions required during its preparation. Nonetheless, the microbiology laboratory used ensured a proper setting for such analysis given the good

tracking of calibrated equipment. Currently there are no other available or validated techniques for a pyrogen assay, however, a promissory version of the LAL based on optical differentiation of the gel formation is been developed and would greatly alleviate the time consumption of the current technique.

Regarding the mathematical models reviewed, those relating osmotic pressure to operational parameters proved to be the most applicable for the investigation performed. Those based on properties of the boundary layer around the membrane would have required more precise technology to measure retained accumulations of endotoxins. In addition, such evaluations to assess other models would require membrane destruction, a non-practical approach for ceramic membranes due to their mechanical properties and costs.

Nonetheless, the osmotic pressure calculations completed for the operational parameters studied are a fair starting point for later investigation and comparison. No information regarding osmotic pressure of endotoxin ultrafiltration was readily available in current literature. In general, the factors that can lead to flux variations according to the osmotic model are:

1. High permeate fluxes, obtained by a large applied pressure or a small membrane resistance
2. Bulk concentrations, which can overcome the back diffusion of solutes from the membrane back to the bulk generating concentration polarization.

3. A small diffusion coefficient of the solute (a macromolecular solute like endotoxin aggregates) and/or a low degree of mechanical mixing near the membrane interface such as in laminar and transition flows

In conclusion, the desired high degree of concentration of pyrogenic solutions, obtained at high volumetric feed rates, appears to be opposed by the same flux and concentration, although the concentrations studied allowed for acceptable permeate fluxes with no pyrogenic content. However, confidence in the model estimates for osmotic pressure is low given the uncertainties occurring from the logarithmic fitting of the experimental data. Therefore, future studies should assess the mass balance of endotoxins around the entire experimental system to better understand the build up characteristics around the membrane interface in terms of conformation, thickness and compressibility. Currently there is not urgent need of such investigation given that fouling of ceramic membranes used for water depyrogenation is well prevented by routine cleaning and sterilization procedures.

## VI. RECOMMENDATIONS

The following is a listing of recommendations extracted from different points during course of this study. They are intended to ease future investigational endeavors on the subject matter of this script and also to expand the research of ceramic membranes used in water depyrogenation.

- Technology for flow measurements has evolved enough to avoid usage of manual float meters, which have a high degree of variability given their human visual component. Usage of electronic instruments such as magnetic or turbine flow meters are currently affordable options for similar studies.
- A great degree of skill is required to master the LAL method to determine endotoxin concentration in addition multiple dilutions are required to accommodate a standard of reference with sensitivity 0.03 EU/mL. Hereby it is recommended that lower sensitivity standards are use for a similar investigation (0.25 EU/mL) to avoid excessive dilution. Also, direct assistance from experimented microbiologists is learning the laboratory techniques are encouraged.
- Given the limited resources for this investigation, no optical techniques were used to investigate the surface conditions of the ceramic membrane after operation. Hereby it is recommended that future researchers would come up with visual depictions of the membrane conditions upon completion of experimental trials. Various microscopy techniques could be applied.

- Long-term fouling effect on ceramic membranes is still a subject of investigation.

Studies on this respect are also recommended.

## VII. BIBLIOGRAPHY

- <sup>1</sup> Bakjer, R.J. Fane, A. Fell, C. and Yoo, B. 1985, Factors affecting flux in crossflow filtration., *Desalination*, 53, pages 81-93.
- <sup>2</sup> Cheryan, M. 1986. *Ultrafiltration Handbook*. Technomic Publishing, Pennsylvania, pages Preface, 4, 7 and 246.
- <sup>3</sup> Engel, M. A., Cheung, V. 1994. *Water For Injection Production Using Ceramic Membrane Technology: Validation Study*. Merck Sharp & Dohme, West Point, PA.
- <sup>4</sup> Elzo, D., Schmitz, P., Houi, D. and S. Joscelyne. 1996. Measurement of particle/membrane interactions by a hydrodynamic method. *Journal of Membrane Science* No. 109: pages 43-53.
- <sup>5</sup> Howell, J. A. and Velincangil, O. 1980, Theoretical considerations of membrane fouling and its treatment with immobilized enzymes for protein ultrafiltration, *Polymer Science and Technology*, Vol 13, Plenum Press, new York, NY, pages 217-229
- <sup>6</sup> Ilias, Shumsuddin, and R. Govind. 1989. Simulation of flux decline due to particulate fouling in ultrafiltration. *Particulate Science and Technology* Vol. 7: pages 187-199.
- <sup>7</sup> Jonsson , Ann-Sofi. 1995. Concentration polarization and fouling during ultrafiltration of colloidal suspensions and hydrophobic solutes. *Separation Science and Technology* 30(2): pages 301-312.
- <sup>8</sup> Krygier, Vivien and Hauhney, Holly, 1997 “Ultrafiltration in the Production of Pyrogen-Free Water”, *Ultrapure Water*.
- <sup>9</sup> Kunihiro, Y. 1989 “Water for Injection Produced by Reverse Osmosis and Ultrafiltration Membrane”. Meiji-Kinenkan, Tokyo Japan.
- <sup>10</sup> Lindau, J., Jonsson, A. S. and R. Wimmerstedt. 1995. The influence of a low-molecular hydrophobic solute on the flux of polysulphone ultrafiltration membranes with different cut-off. *Journal of Membrane Science* No. 106: pages 9-16.
- <sup>11</sup> Novitsky, Thomas J. 1984. *Monitoring and Validation of High Purity Water Systems with the Limulus Amebocyte Lysate Test for Pyrogens*, Associates of Cape Cod, Inc.
- <sup>12</sup> Parekh, B. S. 1991. Get your process water to come clean. *Chemical Engineering Magazine*, January 1991: pages 80-91.

**VII BIBLIOGRAPHY (continued)**

<sup>13</sup> Porter, Mark C. 1990. Handbook of Industrial Membrane Technology. Noyes Publications, New Jersey, pages 161 and 216.

<sup>14</sup> Van Den Berg, G.B.; Smolders, CA.; 1990, Flux Decline in Ultrafiltration Processes; Desalination, 77, pages 101-133

## APPENDIX

Appendix 1. Design parameters for the Membralox® experimental element as provided by vendor literature.

<i>Design Parameters</i>	<i>Values (Max / Min.)</i>	<i>Units</i>
Membrane Surface Area	0.0055	m <sup>2</sup>
Membrane Inner Diameter	0.007	m
Membrane Outer Diameter	0.01	m
Membrane Length	0.25	m
Acidic Resistance	0 / 14	pH
Pore size	0.02	μm
Molecular weight cut off	20,000 / 50,000	Dalton
Material of construction (membrane on support)	ZrO <sub>2</sub> on α-Al <sub>2</sub> O <sub>3</sub>	NA
Pressure	NA	NA
Membrane	115	psig
System	70	psig
Temperature	NA	NA
Membrane	225	°C
System	100	°C
Permeate Range	0.005 / 0.15 (54.5 / 1636)	L/min (L/m <sup>2</sup> ·hr)

Appendix 2. Flow rates studied and the corresponding Reynolds # for the Membralox® experimental element.

<i>Flow rate (mL/min)</i>	<i>Reynolds No. (25 to 30 °C)</i>
150	926 to 1031
250	1543 to 1718
375	2314 to 2578
500	3086 to 3437
625	3857 to 4296
750	4628 to 5155
1250	7714 to 8592
1890	11664 to 12991
3780	23327 to 25983
5670	34991 to 38974
7560	46655 to 51966
9450	58318 to 64957

Appendix 3. Permeate flux raw data for &lt; 0.03 EU/mL water.

$P_{TM}$ (psig)	@ 250 mL/min		@ 375 mL/min		@ 500 mL/min		@ 625 mL/min	
	gph	L/(m <sup>2</sup> .hr)						
5	0.1	51.5	0.1	68.7	0.1	51.5	0.1	61.9
10	0.2	103.1	0.2	130.6	0.2	103.1	0.2	103.1
15	0.3	178.7	0.3	206.2	0.2	164.9	0.3	171.8
20	0.4	240.5	0.4	274.9	0.4	261.2	0.4	261.2
25	0.5	316.1	0.6	412.4	0.5	343.6	0.5	309.3
30	0.6	412.4	0.7	481.1	0.6	412.4	0.6	412.4
35	ND	ND	0.8	515.5	0.7	481.1	0.7	481.1
40	ND	ND	0.8	549.8	0.8	515.5	0.8	549.8
45	ND	ND	0.9	618.5	0.9	584.2	0.9	618.5
50	ND	ND	1.0	687.3	1.0	652.9	1.0	687.3

$P_{TM}$ (psig)	@ 750 mL/min		@ 1250 mL/min		@ 7760 mL/min		@ 9450 mL/min	
	gph	L/(m <sup>2</sup> .hr)	gph	L/(m <sup>2</sup> .hr)	Gph	L/(m <sup>2</sup> .hr)	gph	L/(m <sup>2</sup> .hr)
5	0.1	55.0	0.1	55.0	0.1	34.4	0.1	68.7
10	0.2	103.1	0.2	103.1	0.3	189.0	0.3	171.8
15	0.3	171.8	0.3	206.2	0.4	274.9	0.5	326.5
20	0.4	274.9	0.4	274.9	0.5	343.6	0.6	412.4
25	0.5	329.9	0.6	412.4	0.6	412.4	0.8	515.5
30	0.6	412.4	0.7	481.1	0.8	515.5	ND	ND
35	0.7	481.1	0.8	515.5	1.0	652.9	ND	ND
40	0.8	515.5	0.9	584.2	1.0	652.9	ND	ND
45	0.8	549.8	0.9	618.5	1.0	687.3	ND	ND
50	1.0	687.3	1.0	687.3	1.3	859.1	ND	ND

Appendix 4. Average permeate flux results and Standard Error (SE) in L/(m<sup>2</sup>.hr) for < 0.03 EU/mL water at 25-30 °C.

<i>PTM (psig)</i>	<i>Laminar</i>	<i>Laminar SE</i>	<i>Transition</i>	<i>Transition SE</i>	<i>Turbulent</i>	<i>Turbulent SE</i>
5	51.55	ND	60.71	4.99	49.48	6.66
10	103.09	ND	112.25	9.16	154.64	21.73
15	178.69	ND	180.98	12.76	250.85	27.49
20	240.55	ND	265.75	4.58	329.89	25.72
25	316.15	ND	355.09	30.31	416.49	29.45
30	412.36	ND	435.27	22.91	481.09	24.30
35	ND	ND	492.55	11.45	584.18	50.58
40	ND	ND	538.36	11.45	584.18	39.68
45	ND	ND	607.09	11.45	618.55	39.68
50	ND	ND.	675.82	11.45	744.55	57.27

Appendix 5. Permeate flux raw data for 100 EU/mL water (Data set No. 1).

$P_{TM}$ ( <i>psig</i> )	@ 150 mL/min		@ 250 mL/min		@ 375 mL/min		@ 750 mL/min	
	<i>gph</i>	L/(m <sup>2</sup> .hr)						
5	0.100	68.727	0.075	51.545	0.090	61.855	0.075	51.545
10	0.180	123.709	0.170	116.836	0.160	109.964	0.140	96.218
15	0.290	199.309	0.250	171.818	0.280	192.436	0.230	158.073
20	0.450	309.273	0.400	274.909	0.400	274.909	0.380	261.164
25	0.600	412.364	0.550	378.000	0.500	343.637	0.500	343.637
30	0.700	481.091	0.650	446.727	0.600	412.364	0.600	412.364
35	ND	ND	0.700	481.091	0.750	515.455	0.700	481.091
40	ND	ND	0.750	515.455	0.800	549.818	0.800	549.818
45	ND	ND	0.950	652.909	0.950	652.909	0.900	618.546
50	ND	ND	1.000	687.273	1.000	687.273	1.000	687.273

$P_{TM}$ ( <i>psig</i> )	@ 5678 mL/min		@ 7760 mL/min		@ 9450 mL/min	
	<i>gph</i>	L/(m <sup>2</sup> .hr)	<i>Gph</i>	L/(m <sup>2</sup> .hr)	<i>gph</i>	L/(m <sup>2</sup> .hr)
5	0.05	34.36	0.05	34.36	0.05	34.36
10	0.18	120.27	0.19	130.58	0.15	103.09
15	0.30	206.18	0.38	257.73	0.30	206.18
20	0.48	326.45	0.50	343.64	0.45	309.27
25	0.60	412.36	0.60	412.36	0.55	378.00
30	0.75	515.45	0.75	515.45	0.75	515.45
35	0.85	584.18	0.90	618.55	0.80	549.82
40	1.00	687.27	1.00	687.27	0.90	618.55
45	1.10	756.00	1.25	859.09	1.00	687.27
50	1.50	1030.91	1.50	1030.91	1.25	859.09

Appendix 6. Permeate flux raw data for 100 EU/mL water (Data set No. 2).

$P_{TM}$ ( <i>psig</i> )	@ 150 mL/min		@ 250 mL/min		@ 375 mL/min		@ 750 mL/min	
	<i>gph</i>	L/(m <sup>2</sup> .hr)						
5	0.050	34.364	0.075	51.545	0.075	51.545	0.075	51.545
10	0.150	103.091	0.170	116.836	0.150	103.091	0.180	123.709
15	0.220	151.200	0.270	185.564	0.270	185.564	0.300	206.182
20	0.320	219.927	0.370	254.291	0.390	268.036	0.450	309.273
25	0.420	288.655	0.500	343.637	0.480	329.891	0.550	378.000
30	0.480	329.891	0.600	412.364	0.600	412.364	0.700	481.091
35	0.750	515.455	0.720	494.837	0.700	481.091	0.750	515.455
40	0.800	549.818	0.800	549.818	0.780	536.073	0.800	549.818
45	0.820	563.564	0.850	584.182	0.800	549.818	0.900	618.546
50	0.950	652.909	1.000	687.273	0.900	618.546	1.000	687.273

Appendix 7. Averaged permeate flux results and standard errors (SE) in L/(m<sup>2</sup>.hr) for 100 EU/mL water at 25-30 °C for different flow regions.

<i>PTM (psig)</i>	<i>Laminar</i>	<i>Laminar SE</i>	<i>Transition</i>	<i>Transition SE</i>	<i>Turbulent</i>	<i>Turbulent SE</i>
5	51.55	8.59	56.70	5.15	41.24	4.21
10	114.55	5.25	106.53	3.44	114.77	6.48
15	178.69	12.39	189.00	3.44	206.87	15.76
20	261.16	22.53	271.47	3.44	309.96	13.76
25	348.22	30.99	336.76	6.87	391.75	13.75
30	423.82	26.25	412.36	0.00	487.96	20.04
35	505.15	8.42	498.27	17.18	549.82	24.30
40	542.95	5.61	542.95	6.87	618.55	30.74
45	573.87	8.42	601.36	51.55	707.89	45.59
50	670.09	14.03	652.91	34.36	859.09	76.84

Appendix 8. Permeate flux raw data for 500 EU/mL water (Data set No. 1).

$P_{TM}$ ( <i>psig</i> )	@ 250 mL/min		@ 375 mL/min		@ 750 mL/min	
	<i>gph</i>	L/(m <sup>2</sup> .hr)	<i>Gph</i>	L/(m <sup>2</sup> .hr)	<i>Gph</i>	L/(m <sup>2</sup> .hr)
5	0.09	61.855	0.09	61.855	0.05	34.364
10	0.17	116.836	0.16	109.964	0.15	103.091
15	0.28	192.436	0.26	178.691	0.23	158.073
20	0.39	268.036	0.40	274.909	0.37	254.291
25	0.50	343.637	0.50	343.637	0.50	343.637
30	0.60	412.364	0.60	412.364	0.60	412.364
35	0.75	515.455	0.75	515.455	0.70	481.091
40	0.80	549.818	0.80	549.818	0.80	549.818
45	0.90	618.546	0.90	618.546	0.85	584.182
50	0.95	652.909	1.00	687.273	0.95	652.909

$P_{TM}$ ( <i>psig</i> )	@ 5678 mL/min		@ 7760 mL/min		@ 9450 mL/min	
	<i>gph</i>	L/(m <sup>2</sup> .hr)	<i>Gph</i>	L/(m <sup>2</sup> .hr)	<i>gph</i>	L/(m <sup>2</sup> .hr)
5	0.10	68.73	0.05	34.36	0.05	34.36
10	0.20	137.45	0.20	137.45	0.15	103.09
15	0.33	223.36	0.25	171.82	0.25	171.82
20	0.45	309.27	0.40	274.91	0.38	257.73
25	0.60	412.36	0.50	343.64	ND	ND
30	ND	ND	ND	ND	ND	ND
35	ND	ND	ND	ND	ND	ND
40	ND	ND	ND	ND	ND	ND
45	ND	ND	ND	ND	ND	ND
50	ND	ND	ND	ND	ND	ND

Appendix 9. Permeate flux raw data for 500 EU/mL water (Data set No. 2).

$P_{TM}$ ( <i>psig</i> )	@ 150 mL/min		@ 250 mL/min		@ 375 mL/min		@ 750 mL/min	
	<i>Gph</i>	L/(m <sup>2</sup> .hr)						
5	0.08	51.55	0.08	51.55	0.05	34.36	0.05	34.36
10	0.15	103.09	0.17	116.84	0.13	89.35	0.13	89.35
15	0.22	151.20	0.22	151.20	0.20	137.45	0.23	158.07
20	0.35	240.55	0.40	274.91	0.25	171.82	0.33	226.80
25	0.45	309.27	0.45	309.27	0.42	288.65	0.48	329.89
30	0.65	446.73	0.60	412.36	0.50	343.64	0.55	378.00
35	0.70	481.09	0.70	481.09	0.70	481.09	0.68	467.35
40	0.75	515.45	0.75	515.45	0.72	494.84	0.75	515.45
45	0.85	584.18	0.80	549.82	0.77	529.20	0.80	549.82
50	0.90	618.55	0.95	652.91	0.85	584.18	0.90	618.55

Appendix 10. Averaged permeate flux results and standard error (SE) in L/(m<sup>2</sup>.hr) for 500 EU/mL water at 25-30 °C for different flow regions.

<i>PTM (psig)</i>	<i>Laminar</i>	<i>Laminar SE</i>	<i>Transition</i>	<i>Transition SE</i>	<i>Turbulent</i>	<i>Turbulent SE</i>
5	54.98	3.44	34.36	13.75	41.24	6.87
10	112.25	4.58	89.35	10.31	114.09	9.86
15	164.95	13.75	137.45	20.62	176.63	12.08
20	261.16	10.50	171.82	51.55	264.60	13.57
25	320.73	11.45	288.65	27.49	357.38	18.61
30	423.82	11.45	343.64	34.36	395.18	17.18
35	492.55	11.45	481.09	17.18	474.22	4.35
40	526.91	11.45	494.84	27.49	532.64	10.87
45	584.18	19.84	529.20	44.67	567.00	10.87
50	641.45	11.45	584.18	51.55	635.73	10.87

Appendix 11. Permeate flux raw data for 667 EU/mL water (Data set No. 1).

$P_{TM}$ ( <i>psig</i> )	@ 250 mL/min		@ 375 mL/min		@ 750 mL/min	
	<i>gph</i>	L/(m <sup>2</sup> .hr)	<i>Gph</i>	L/(m <sup>2</sup> .hr)	<i>gph</i>	L/(m <sup>2</sup> .hr)
5	0.08	51.55	0.05	34.36	0.05	34.36
10	0.13	89.35	0.11	75.60	0.13	89.35
15	0.18	123.71	0.16	109.96	0.18	123.71
20	0.25	171.82	0.25	171.82	0.25	171.82
25	0.33	226.80	0.33	226.80	0.35	240.55
30	0.45	309.27	0.45	309.27	0.45	309.27
35	0.50	343.64	0.50	343.64	0.50	343.64
40	0.60	412.36	0.60	412.36	0.60	412.36
45	0.70	481.09	0.70	481.09	0.70	481.09
50	0.75	515.45	0.75	515.45	0.75	515.45

$P_{TM}$ ( <i>psig</i> )	@ 3780 mL/min		@ 9450 mL/min		@ 9450 mL/min	
	<i>gph</i>	L/m <sup>2</sup> *hr	<i>Gph</i>	L/(m <sup>2</sup> .hr)	<i>gph</i>	L/(m <sup>2</sup> .hr)
5	0.08	51.55	0.10	68.73	0.09	61.85
10	0.20	137.45	0.20	137.45	0.20	137.45
15	0.35	240.55	0.55	378.00	0.30	206.18
20	0.50	343.64	0.55	378.00	0.50	343.64
25	0.70	481.09	0.70	481.09	0.70	481.09
30	0.80	549.82	0.80	549.82	0.75	515.45
35	1.00	687.27	ND	ND	ND	ND
40	ND	ND	ND	ND	ND	ND
45	ND	ND	ND	ND	ND	ND
50	ND	ND	ND	ND	ND	ND

Appendix 12. Permeate flux raw data for 667 EU/mL water (Data set No. 2).

$P_{TM}$ ( <i>psig</i> )	@ 150 mL/min		@ 250 mL/min		@ 375 mL/min		@ 750 mL/min	
	<i>Gph</i>	L/(m <sup>2</sup> .hr)						
5	0.05	34.36	0.08	51.55	0.05	34.36	0.08	51.55
10	0.15	103.09	0.15	103.09	0.15	103.09	0.15	103.09
15	0.21	144.33	0.22	151.20	0.20	137.45	0.22	151.20
20	0.30	206.18	0.30	206.18	0.32	219.93	0.37	254.29
25	0.41	281.78	0.43	295.53	0.43	295.53	0.48	329.89
30	0.55	378.00	0.55	378.00	0.52	357.38	0.60	412.36
35	0.65	446.73	0.65	446.73	0.65	446.73	0.70	481.09
40	0.70	481.09	0.70	481.09	0.70	481.09	0.75	515.45
45	0.80	549.82	0.80	549.82	0.75	515.45	0.85	584.18
50	0.85	584.18	0.85	584.18	0.80	549.82	0.90	618.55

Appendix 13. Averaged permeate flux results and standard error (SE) in L/(m<sup>2</sup>.hr) for 667 EU/mL water at 25-30 °C for different flow regions.

<i>PTM (psig)</i>	<i>Laminar</i>	<i>Laminar SE</i>	<i>Transition</i>	<i>Transition SE</i>	<i>Turbulent</i>	<i>Turbulent SE</i>
5	45.82	5.73	34.36	0.00	53.61	5.81
10	98.51	4.58	75.60	13.75	120.96	10.33
15	139.75	8.26	109.96	13.75	219.93	44.49
20	194.73	11.45	171.82	24.05	298.28	37.68
25	268.04	21.00	226.80	34.36	402.74	50.02
30	355.09	22.91	309.27	24.05	467.35	46.87
35	412.36	34.36	343.64	51.55	504.00	99.86
40	458.18	22.91	412.36	34.36	463.91	51.55
45	526.91	22.91	481.09	17.18	532.64	51.55
50	561.27	22.91	515.45	17.18	567.00	51.55

Appendix 14. Two-Sample T-Test of Membrane Resistance at the Laminar and Transition Reynolds Regions

$N_{Re}$	$N$	$Mean$	$StDev$	$SE$
[926, 2578]	10	2193000000	196471655	62129792
[3086, 5155]	10	2333000000	249223238	78811308

Difference =  $\mu_{Re} = [926,2578] - \mu_{Re} = [3086, 5155]$

Estimate for difference: -140000000

95% upper bound for difference: 34580031

T-Test of difference = 0 (vs <): T-Value = -1.40 **P-Value = 0.090** DF = 17

Appendix 15. Two-way ANOVA of the Membrane Resistance with Pressure and Flow Region Factors

Factors	DF	SS	MS	F	P
Reynolds	2	1.215E+18	6.074E+17	37.50	0.000
P transm	2	3.228E+17	1.614E+17	9.97	0.001
Interaction	4	2.394E+17	5.984E+16	3.69	0.023
Error	18	2.915E+17	1.620E+16		
Total	26	2.069E+18			

Individual 95% CI

Reynolds	Mean	-----+-----+-----+-----+-----
Laminar	2301111111	(---*---)
Turbulent	1797777778	(----*---)
Transition	2161111111	(---*---)
		-----+-----+-----+-----+-----
		1.80E+09 2.00E+09 2.20E+09 2.40E+09

Individual 95% CI

P transm	Mean	-----+-----+-----+-----+-----
1	2218888889	(-----*-----)
2	1951111111	(-----*-----)
3	2090000000	(-----*-----)
		-----+-----+-----+-----+-----
		1.92E+09 2.04E+09 2.16E+09 2.28E+09

Appendix 16. Linear regression results for <0.03 EU/mL feed concentration at laminar flow rate.

<i>Regression Statistics</i>	
Multiple R	0.9961
R Square	0.9923
Adjusted R Square	0.9913
Standard Error	19.6368
Observations	10

<i>Source of Variation</i>	<i>df</i>	<i>SS</i>	<i>MS</i>	<i>F</i>	<i>Significance F</i>
<i>Regression</i>	1	396563.03	396563.03	1028.42	9.73681E-10
<i>Residual</i>	8	3084.83	385.60	NA	NA
<i>Total</i>	9	399647.86	NA	NA	NA

	<i>Coefficients</i>	<i>Standard Error</i>	<i>t Stat</i>	<i>P-value</i>	<i>Lower 95%</i>	<i>Upper 95%</i>
Intercept	-10.68	13.41	-0.80	0.45	-41.61	20.26
PTM (psig)	13.87	0.43	32.07	0.00	12.87	14.86

## Appendix 16. (Continued)

$P_{TM}$ (psig)	Fitted values of regression	RESIDUAL OUTPUT	
		Laminar feed rate	Transition feed rate
5	58.66	1.82	0.62
10	127.99	-13.90	-19.74
15	197.32	-15.88	-18.63
20	266.65	-8.23	4.82
25	335.98	11.78	-0.94
30	405.31	33.17	24.23
35	474.64	27.07	15.04
40	543.97	-2.75	-16.49
45	613.31	-11.94	-20.53
50	682.64	-21.14	-3.95

$P_{TM}$ (psig)	Fitted values of regression	RESIDUAL OUTPUT	
		Laminar feed rate	Transition feed rate
5	53.14	3.56	-1.59
10	125.52	-12.12	-29.30
15	197.90	-15.78	-39.83
20	270.29	4.62	-9.12
25	342.67	18.15	0.97
30	415.05	14.50	-2.69
35	487.43	10.84	-6.34
40	559.82	-27.18	-10.00
45	632.20	20.71	-13.65
50	704.58	-17.31	-17.31

Appendix 17. Linear regression results for 100 EU/mL feed concentration.

<i>Regression Statistics</i>	
Multiple R	0.993
R Square	0.986
Adjusted R Square	0.986
Standard Error	24.546
Observations	20.000

<i>Source of Variation</i>	<i>df</i>	<i>SS</i>	<i>MS</i>	<i>F</i>	<i>Significance F</i>
<i>Regression</i>	1	787299.74	787299.74	1306.67	2.94742E-18
<i>Residual</i>	18	10845.46	602.53	NA	NA
<i>Total</i>	19	798145.20	NA	NA	NA

	<i>Coefficients</i>	<i>Standard Error</i>	<i>t Stat</i>	<i>P-value</i>	<i>Lower 95%</i>	<i>Upper 95%</i>
Intercept	-14.55	11.86	-1.23	0.24	-39.46	10.36
P <sub>TM</sub> (psig)	13.82	0.38	36.15	0.00	13.01	14.62

## Appendix 17. (Continued)

$P_{TM}$ (psig)	Fitted values of regression	RESIDUAL OUTPUT	
		Laminar feed rate	Transition feed rate
5	54.53	-11.57	-2.98
10	123.61	-13.64	-10.20
15	192.68	-24.30	3.19
20	261.76	-24.65	26.90
25	330.83	-14.69	40.29
30	399.91	-4.73	46.82
35	468.99	36.16	29.29
40	538.06	4.88	4.88
45	607.14	-33.27	-22.96
50	676.21	-6.12	-23.30

$P_{TM}$ (psig)	Fitted values of regression	RESIDUAL OUTPUT	
		Laminar feed rate	Transition feed rate
5	48.42	13.43	-14.06
10	118.95	-5.55	-15.86
15	189.48	-3.92	-31.41
20	260.01	11.46	-5.72
25	330.54	13.10	13.10
30	401.07	11.30	11.30
35	471.59	43.86	9.50
40	542.12	7.70	7.70
45	612.65	5.89	-28.47
50	683.18	-13.09	-30.27

Appendix 18. Linear regression results for 500 EU/mL feed concentration.

<i>Regression Statistics</i>	
Multiple R	0.99
R Square	0.98
Adjusted R Square	0.98
Standard Error	26.36
Observations	20.00

<i>Source of Variation</i>	<i>df</i>	<i>SS</i>	<i>MS</i>	<i>F</i>	<i>Significance F</i>
<i>Regression</i>	1.00	732391.19	732391.19	1054.02	1.98E-17
<i>Residual</i>	18.00	12507.39	694.85	NA	NA
<i>Total</i>	19.00	744898.57	NA	NA	NA

	<i>Coefficients</i>	<i>Standard Error</i>	<i>t Stat</i>	<i>P-value</i>	<i>Lower 95%</i>	<i>Upper 95%</i>
Intercept	-27.95	12.73	-2.19	0.04	-54.70	-1.20
P <sub>TM</sub> (psig)	13.32	0.41	32.47	0.00	12.46	14.19

## Appendix 18. (Continued)

$P_{TM}$ (psig)	<i>Fitted values of regression</i>	<i>RESIDUAL OUTPUT</i>	
		<i>Laminar feed rate</i>	<i>Transition feed rate</i>
5	38.67	12.87	-4.31
10	105.30	4.67	-15.95
15	171.92	-20.72	-24.16
20	238.55	19.18	-39.24
25	305.17	4.10	4.10
30	371.79	57.75	-10.98
35	438.42	42.67	35.80
40	505.04	10.41	0.10
45	571.67	-4.67	-32.16
50	638.29	-2.56	-36.93

Appendix 19. Linear regression results for 667 EU/mL feed concentration.

<i>Regression Statistics</i>	
Multiple R	0.997
R Square	0.994
Adjusted R Square	0.994
Standard Error	12.766
Observations	20.000

<i>Source of Variation</i>	<i>Df</i>	<i>SS</i>	<i>MS</i>	<i>F</i>	<i>Significance F</i>
<i>Regression</i>	1.00	502,865.88	502,865.88	3,085.39	1.38147E-21
<i>Residual</i>	18.00	2,933.70	162.98	NA	NA
<i>Total</i>	19.00	505,799.58	NA	NA	NA

	<i>Coefficients</i>	<i>Standard Error</i>	<i>t Stat</i>	<i>P-value</i>	<i>Lower 95%</i>	<i>Upper 95%</i>
Intercept	-32.42	6.17	-5.26	5.35E-05	-45.37	-19.46
P <sub>TM</sub> (psig)	11.04	0.20	55.55	1.38E-21	10.62	11.46

## Appendix 19. (Continued)

$P_{TM}$ (psig)	Fitted values of regression	RESIDUAL OUTPUT	
		Laminar feed rate	Transition feed rate
5	22.79	20.17	11.57
10	78.00	4.48	11.35
15	133.20	-16.36	-9.49
20	188.41	-16.59	-16.59
25	243.61	-16.81	-3.07
30	298.82	10.45	10.45
35	354.02	-10.39	-10.39
40	409.23	3.13	3.13
45	464.44	16.66	16.66
50	519.64	-4.19	-4.19

Appendix 20. Linear regression results for 667 EU/mL feed concentration (Data set # 2).

<i>Regression Statistics</i>	
Multiple R	0.995
R Square	0.989
Adjusted R Square	0.989
Standard Error	20.036
Observations	20.000

<i>Source of Variation</i>	<i>df</i>	<i>SS</i>	<i>MS</i>	<i>F</i>	<i>Significance F</i>
<i>Regression</i>	1.00	667939.40	667939.40	1663.88	3.43301E-19
<i>Residual</i>	18.00	7225.83	401.43	NA	NA
<i>Total</i>	19.00	675165.22	NA	NA	NA

	<i>Coefficients</i>	<i>Standard Error</i>	<i>t Stat</i>	<i>P-value</i>	<i>Lower 95%</i>	<i>Upper 95%</i>
Intercept	-22.45	9.68	-2.32	0.03	-42.78	-2.12
P <sub>TM</sub> (psig)	12.72	0.31	40.79	3.43E-19	12.07	13.38

## Appendix 20. (Continued)

<i>PTM (psig)</i>	<i>Fitted values of regression</i>	<i>RESIDUAL OUTPUT</i>	
		<i>Laminar feed rate</i>	<i>Transition feed rate</i>
5	41.17	1.78	1.78
10	104.80	-1.71	-1.71
15	168.42	-20.66	-24.10
20	232.05	-25.87	5.06
25	295.67	-7.02	17.04
30	359.30	18.70	25.57
35	422.92	23.80	40.99
40	486.55	-5.46	11.73
45	550.17	-0.35	-0.35
50	613.80	-29.62	-29.62

Appendix 21. Permeate flux data grouped for  $P_{TM}$  of 5 psig (Data set # 1).

<i>Feed Rate Region</i>	<i>Permeate Flux (L/(m<sup>2</sup>.hr))</i>			
	<i>&lt;0.03 EU/mL</i>	<i>100 EU/mL</i>	<i>500 EU/mL</i>	<i>666 EU/mL</i>
<i>Laminar</i>	52.7	56.7	61.9	43.0
<i>Transition</i>	59.3	51.5	34.4	34.4
<i>Turbulent</i>	52.7	34.4	45.8	60.7

Appendix 22. Two-Factor ANOVA results for  $P_{TM}$  of 5 psig (Data set # 1).

<i>SUMMARY</i>	<i>Count</i>	<i>Sum</i>	<i>Average</i>	<i>Variance</i>
<i>Laminar</i>	4	214.2	53.6	64.0
<i>Transition</i>	4	179.6	44.9	157.6
<i>Turbulent</i>	4	193.6	48.4	124.5
<i>&lt;0.03 EU/mL</i>	3	164.7	54.9	14.5
<i>100 EU/mL</i>	3	142.6	47.5	136.8
<i>500 EU/mL</i>	3	142.0	47.3	190.7
<i>666 EU/mL</i>	3	138.0	46.0	180.5

<i>Source of Variation</i>	<i>Sum of Squares</i>	<i>Degrees of Freedom</i>	<i>Mean of Squares</i>	<i>F statistic</i>	<i>P-value</i>	<i>F critical value</i>
<i>Feed rate region</i>	151.9	2.0	75.9	0.5	0.6	5.1
<i>Endotoxin Concentration</i>	145.4	3.0	48.5	0.3	0.8	4.8
<i>Error</i>	893.0	6.0	148.8	NA	NA	NA
<i>Total</i>	1190.3	11.0	NA	NA	NA	NA

Appendix 23. Permeate flux data grouped for  $P_{TM} = 5$  psig (Combined data sets).

<i>Feed Rate Region</i>	<i>Permeate Flux (L/(m<sup>2</sup>.hr))</i>		
	<i>100 EU/mL</i>	<i>500 EU/mL</i>	<i>666 EU/mL</i>
<i>Laminar(Data set # 1)</i>	56.7	61.9	43.0
<i>Laminar(Data set # 2)</i>	43.0	51.5	43.0
<i>Transition (Data set # 1)</i>	51.5	34.4	34.4
<i>Transition (Data set # 2)</i>	51.5	34.4	43.0

Appendix 24. Results of a Two-Factor ANOVA with replications for  $P_{TM} = 5$  psig

<i>Laminar feed rate results summary</i>				
	<i>Count</i>	<i>Sum</i>	<i>Average</i>	<i>Variance</i>
<i>100 EU/mL</i>	2	99.65	49.83	94.47
<i>500 EU/mL</i>	2	113.40	56.70	53.14
<i>666 EU/mL</i>	2	85.91	42.95	0.00
<i>Total</i>	6	298.96	49.83	67.31

<i>Transition feed rate results summary</i>				
	<i>Count</i>	<i>Sum</i>	<i>Average</i>	<i>Variance</i>
<i>100 EU/mL</i>	2	103.09	51.55	0.00
<i>500 EU/mL</i>	2	68.73	34.36	0.00
<i>666 EU/mL</i>	2	77.32	38.66	36.90
<i>Total</i>	6	249.14	41.52	71.34

<i>Source of Variation</i>	<i>Sum of Squares</i>	<i>Degrees of Freedom</i>	<i>Mean of Squares</i>	<i>F statistic</i>	<i>P-value</i>	<i>F critical value</i>
<i>Feed rate region</i>	206.90	1.00	206.90	6.73	0.04	5.99
<i>Endotoxin Concentration</i>	195.33	2.00	97.67	3.18	0.11	5.14
<i>Feed rate / Concentration Interaction</i>	313.42	2.00	156.71	5.10	0.05	5.14
<i>Error</i>	184.51	6.00	30.75	NA	NA	NA
<i>Total</i>	900.16	11.00	NA	NA	NA	NA

Appendix 25. Permeate flux data grouped for  $P_{TM} = 25$  psig (Data set # 1).

<i>Feed Rate Region</i>	<i>Permeate Flux (L/(m<sup>2</sup>.hr))</i>			
	<i>&lt;0.03 EU/mL</i>	<i>100 EU/mL</i>	<i>500 EU/mL</i>	<i>666 EU/mL</i>
<i>Laminar</i>	327.6	360.8	343.6	226.8
<i>Transition</i>	348.8	343.6	343.6	240.5
<i>Turbulent</i>	446.7	400.9	378.0	481.1

Appendix 26. Two-Factor ANOVA results for  $P_{TM} = 25$  psig (Data set # 1).

<i>SUMMARY</i>	<i>Count</i>	<i>Sum</i>	<i>Average</i>	<i>Variance</i>
<i>Laminar</i>	4	1258.86	314.71	3619.01
<i>Transition</i>	4	1276.61	319.15	2752.14
<i>Turbulent</i>	4	1706.73	426.68	2132.11
<i>&lt;0.03 EU/mL</i>	3	1123.12	374.37	4038.65
<i>100 EU/mL</i>	3	1105.36	368.45	863.78
<i>500 EU/mL</i>	3	1065.27	355.09	393.62
<i>666 EU/mL</i>	3	948.44	316.15	20452.50

<i>Source of Variation</i>	<i>Sum of Squares</i>	<i>Degrees of Freedom</i>	<i>Mean of Squares</i>	<i>F statistic</i>	<i>P-value</i>	<i>F critical value</i>
<i>Feed rate region</i>	32158.93	2.00	16079.47	4.99	0.05	5.14
<i>Endotoxin Concentration</i>	6171.61	3.00	2057.20	0.64	0.62	4.76
<i>Error</i>	19338.18	6.00	3223.03	NA	NA	NA
<i>Total</i>	57668.71	11.00	NA	NA	NA	NA

Appendix 27. Permeate flux data grouped for  $P_{TM} = 25$  psig (Combined data sets).

<i>Feed Rate Region</i>	<i>Permeate Flux (L/(m<sup>2</sup>.hr))</i>		
	<i>100 EU/mL</i>	<i>500 EU/mL</i>	<i>666 EU/mL</i>
<i>Laminar(Data set # 1)</i>	360.8	343.6	226.8
<i>Laminar(Data set # 2)</i>	316.1	309.3	288.7
<i>Transition (Data set # 1)</i>	343.6	343.6	240.5
<i>Transition (Data set # 2)</i>	371.1	309.3	312.7

Appendix 28. Results of a Two-Factor ANOVA with replications for  $P_{TM} = 25$  psig .

<i>Laminar feed rate results summary</i>				
	<i>Count</i>	<i>Sum</i>	<i>Average</i>	<i>Variance</i>
<i>100 EU/mL</i>	2.00	676.96	338.48	997.83
<i>500 EU/mL</i>	2.00	652.91	326.45	590.43
<i>666 EU/mL</i>	2.00	515.45	257.73	1912.99
<i>Total</i>	6.00	1845.33	307.55	2218.84

<i>Transition feed rate results summary</i>				
	<i>Count</i>	<i>Sum</i>	<i>Average</i>	<i>Variance</i>
<i>100 EU/mL</i>	2.00	714.76	357.38	377.88
<i>500 EU/mL</i>	2.00	652.91	326.45	590.43
<i>666 EU/mL</i>	2.00	553.25	276.63	2603.80
<i>Total</i>	6.00	1920.93	320.15	2042.49

<i>Source of Variation</i>	<i>Sum of Squares</i>	<i>Degrees of Freedom</i>	<i>Mean of Squares</i>	<i>F statistic</i>	<i>P-value</i>	<i>F critical value</i>
<i>Feed rate region</i>	476.28	1.00	476.28	0.40	0.55	5.99
<i>Endotoxin Concentration</i>	13995.16	2.00	6997.58	5.94	0.04	5.14
<i>Feed rate / Concentration Interaction</i>	238.14	2.00	119.07	0.10	0.91	5.14
<i>Error</i>	7073.35	6.00	1178.89	NA	NA	NA
<i>Total</i>	21782.94	11.00	NA	NA	NA	NA

Appendix 29. Permeate flux data grouped for  $P_{TM} = 50$  psig (Combined data sets).

<i>Feed Rate Region</i>	<i>Permeate Flux (L/(m<sup>2</sup>.hr))</i>		
	<i>100 EU/mL</i>	<i>500 EU/mL</i>	<i>666 EU/mL</i>
<i>Laminar(Data set # 1)</i>	687.3	670.1	515.5
<i>Laminar(Data set # 2)</i>	670.1	635.7	584.2
<i>Transition (Data set # 1)</i>	687.3	652.9	515.5
<i>Transition (Data set # 2)</i>	652.9	601.4	584.2

Appendix 30. Results of a Two-Factor ANOVA with replications for  $P_{TM} = 50$  psig .

<i>Laminar feed rate results summary</i>				
	<i>Count</i>	<i>Sum</i>	<i>Average</i>	<i>Variance</i>
<i>100 EU/mL</i>	2.00	1357.36	678.68	147.61
<i>500 EU/mL</i>	2.00	1305.82	652.91	590.43
<i>666 EU/mL</i>	2.00	1099.64	549.82	2361.72
<i>Total</i>	6.00	3762.82	627.14	4339.66

<i>Transition feed rate results summary</i>				
	<i>Count</i>	<i>Sum</i>	<i>Average</i>	<i>Variance</i>
<i>100 EU/mL</i>	2.00	1340.18	670.09	590.43
<i>500 EU/mL</i>	2.00	1254.27	627.14	1328.47
<i>666 EU/mL</i>	2.00	1099.64	549.82	2361.72
<i>Total</i>	6.00	3694.09	615.68	3827.96

<i>Source of Variation</i>	<i>Sum of Squares</i>	<i>Degrees of Freedom</i>	<i>Mean of Squares</i>	<i>F statistic</i>	<i>P-value</i>	<i>F critical value</i>
<i>Feed rate region</i>	393.62	1.00	393.62	0.32	0.59	5.99
<i>Endotoxin Concentration</i>	33113.29	2.00	16556.65	13.46	0.01	5.14
<i>Feed rate / Concentration Interaction</i>	344.42	2.00	172.21	0.14	0.87	5.14
<i>Error</i>	7380.38	6.00	1230.06	NA	NA	NA
<i>Total</i>	41231.71	11.00	NA	NA	NA	NA